



The essential role of the nature of the binary progenitors for understanding Gamma-Ray Bursts

Remo Ruffini
and collaborators

ICRANet Pescara – Nice – Rio – Rome – Yerevan
Università “La Sapienza” - Rome

$$\frac{Gm}{c^2}$$



Albert Einstein

$$\frac{\hbar}{mc}$$



Max Planck

Pulsars and Neutron stars rotational energy

$$\left(\frac{dE}{dt} \right)_{obs} \simeq 4\pi^2 \frac{I_{NS}}{P^3} \frac{dP}{dt}$$

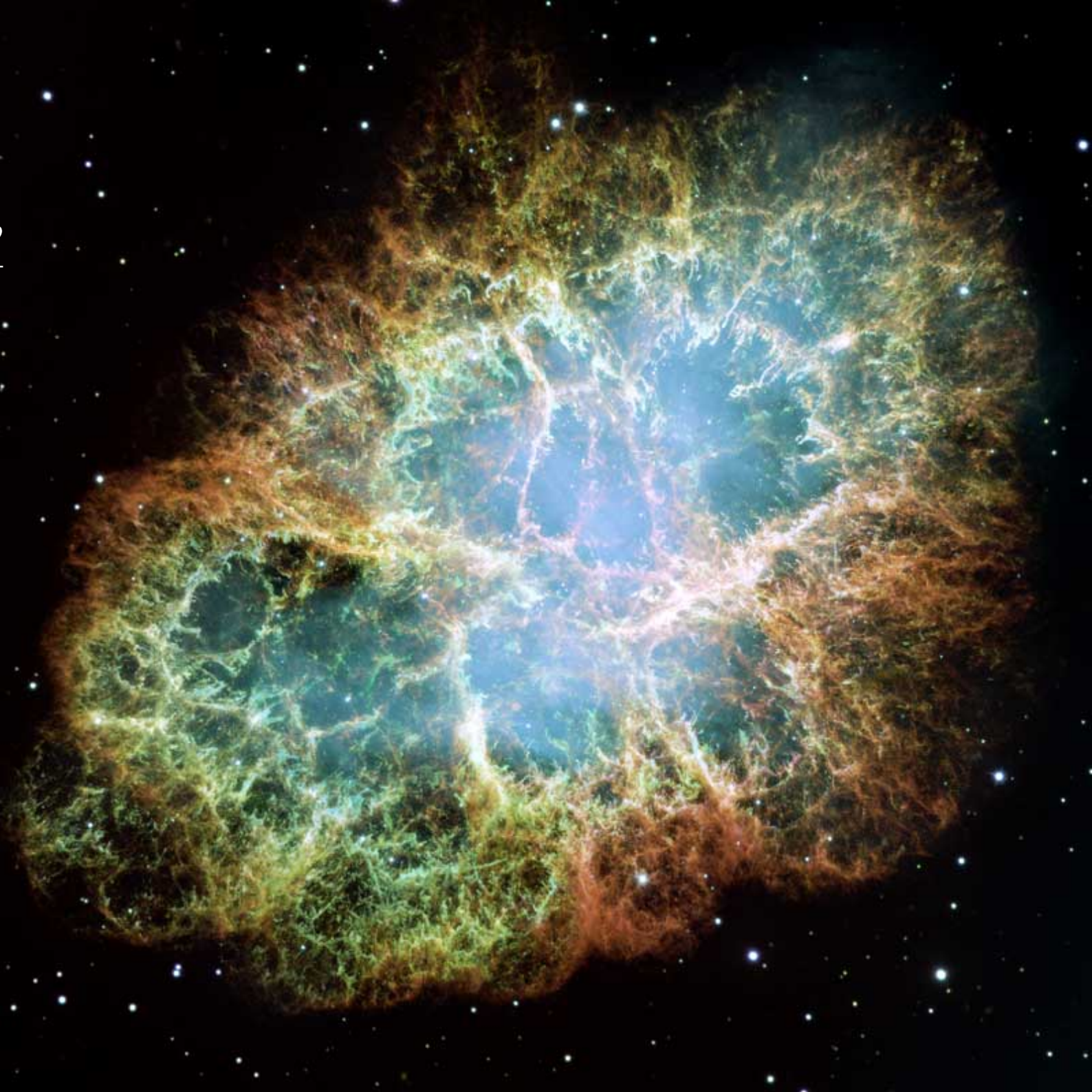
Chinese, Japanese,
Korean astronomers

R. Oppenheimer &
R. Volkoff (1939)

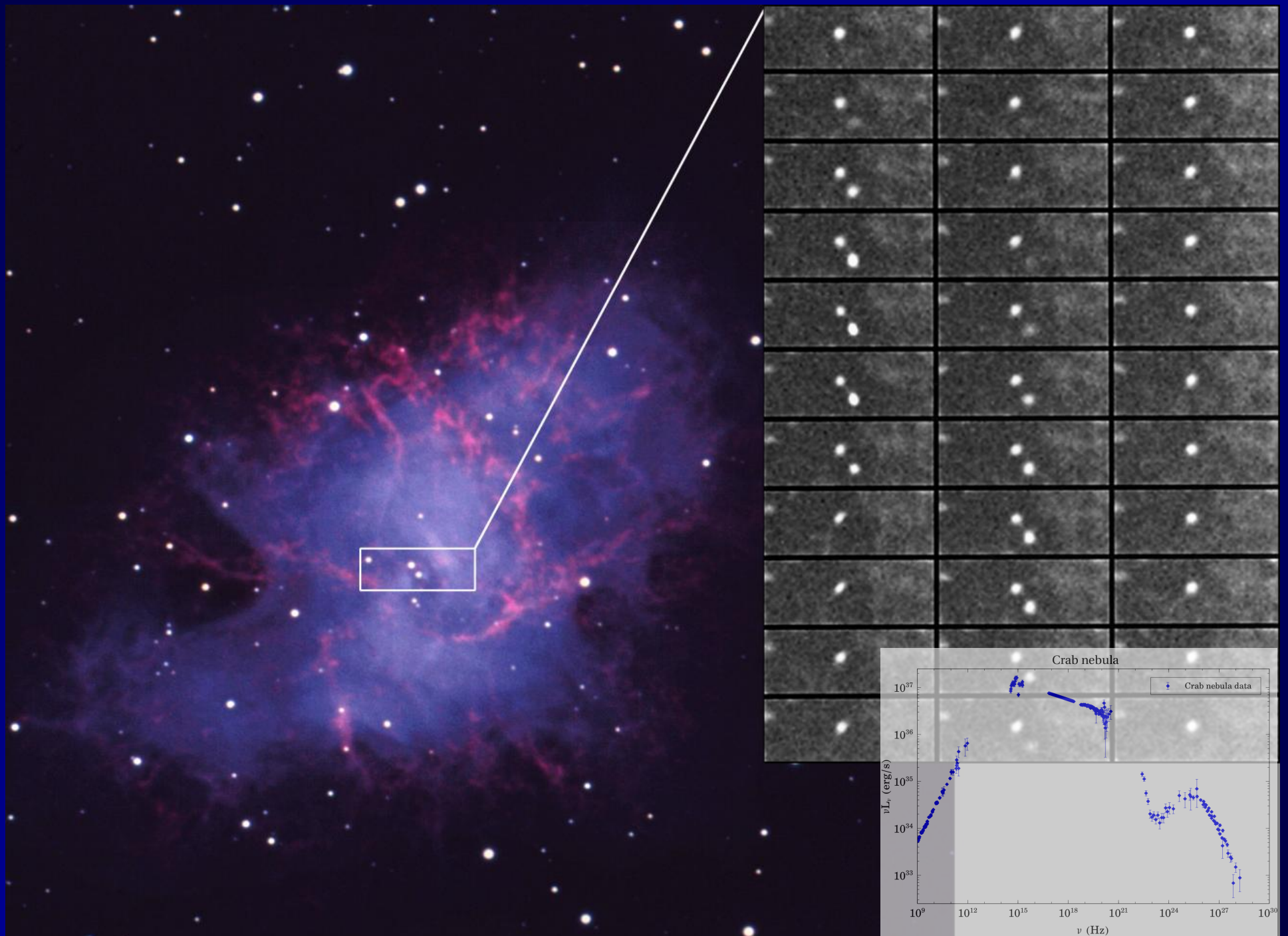
J. Bell & T. Hewish (1967)

UHECRs
(2000-2011)

AGILE Flare (2011)
**Open issue: the emission
of the remnant.**

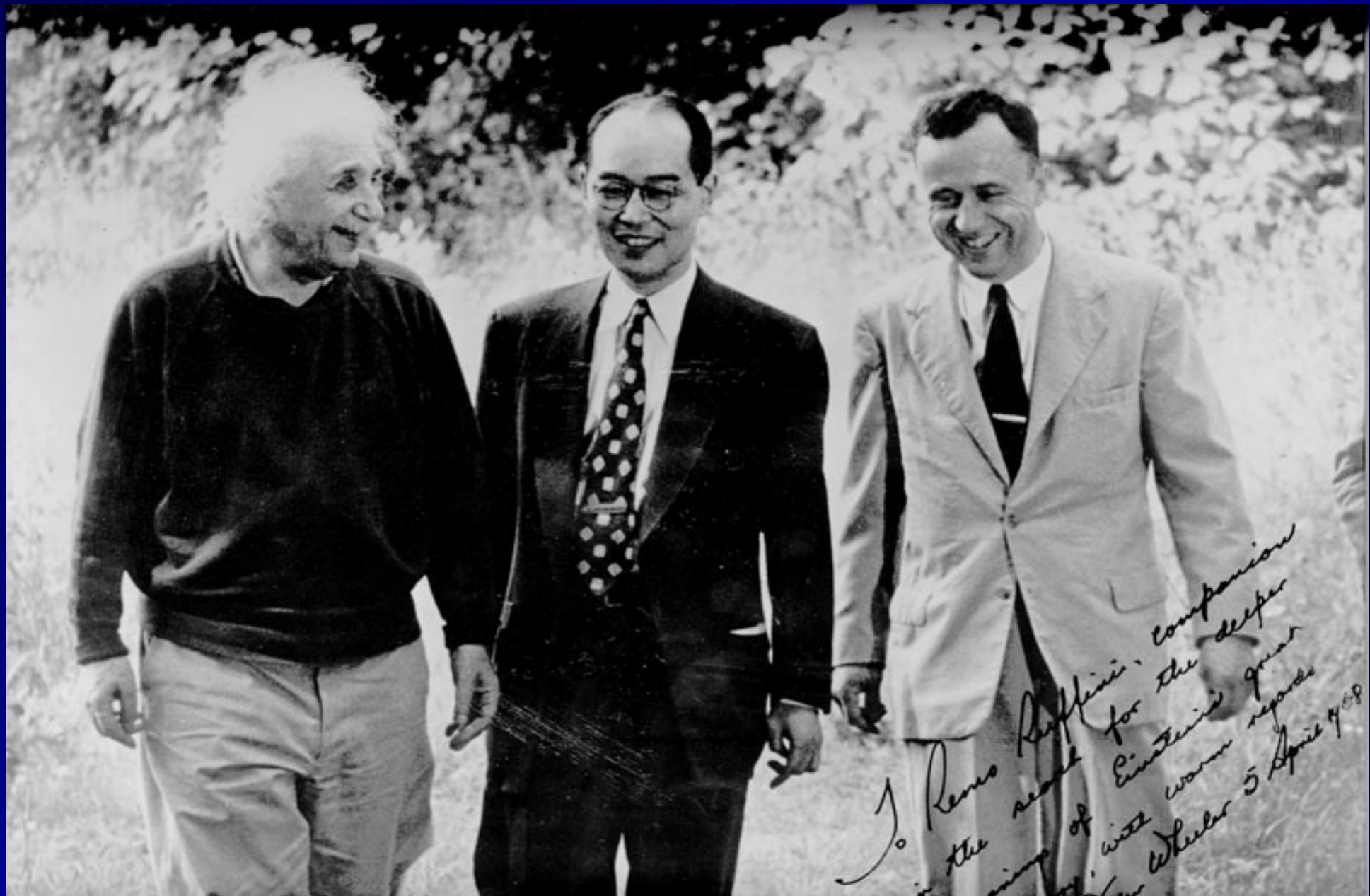


Crab Nebula Pulsar



Einstein, Yukawa and Wheeler: the birth of Relativistic Astrophysics

April 5th, 1968



Princeton, 1971



Joseph Henry Laboratories, Princeton University

Introducing the black hole

According to present cosmology, certain stars end their careers in a total gravitational collapse that transcends the ordinary laws of physics.

Remo Ruffini and John A. Wheeler

The quasistellar object, the pulsar, the neutron star have all come onto the scene of physics within the space of a few years. Is the next entrant destined to be the black hole? If so, it is difficult to think of any development that could be of greater significance. A black hole, whether of "ordinary size" (approximately one solar mass, $1 M_{\odot}$), or much larger (around $10^6 M_{\odot}$ to $10^{10} M_{\odot}$, as proposed in the nuclei of some galaxies) provides our "laboratory model" for the gravitational collapse, predicted by Einstein's theory, of the universe itself.

A black hole is what is left behind after an object has undergone complete gravitational collapse. Spacetime is so strongly curved that no light can come out, no matter can be ejected and no measuring rod can ever survive being put in. Any kind of object that falls into the black hole loses its separate identity, preserving only its mass, charge, angular momentum and linear momentum (see figure 1). No one has yet found a way to distinguish between two black holes constructed out of the most different kinds of matter if they have the same mass, charge and angular momentum. Measurement of these three determinants is permitted by their effect on the Kepler orbits of test objects, charged and uncharged, in revolution about the black hole.

How the physics of a black hole looks depends more upon an act of choice by the observer himself than an anything else. Suppose he decides to follow the collapsing matter through its collapse down into the black hole. Then he will see it crushed to indefi-

nitely high density, and he himself will be torn apart eventually by indefinitely increasing tidal forces. No restraining force whatsoever has the power to hold him away from this catastrophe, once he crossed a certain critical surface known as the "horizon." The final collapse occurs a finite time after the passage of this surface, but it is inevitable. Time and space are interchanged inside a black hole in an unusual way; the direction of increasing proper time for the observer is the direction of decreasing values of the coordinate r . The observer has no more power to return to a larger r value than he has power to turn back the hands on the clock of life itself. He can not even stay where he is, and for a simple reason: no one has the power to stop the advance of time.

Suppose the observer decides instead to observe the collapse from far away. Then, as price for his own safety, he is deprived of any chance to see more than the first steps on the way to collapse. All signals and all information from the later phases of collapse never escape; they are caught up in the collapse of the geometry itself.

That a sufficient mass of cold matter will necessarily collapse to a black hole (J. R. Oppenheimer and H. Snyder,¹) is one of the most spectacular of all the predictions of Einstein's standard 1915 general relativity. The geometry around a collapsed object of spherical symmetry (nonrotating!) was worked out by Karl Schwarzschild of Göttingen, father of the American astrophysicist Martin Schwarzschild, as early as 1916. In 1963 Roy Kerr² found the geometry associated with a rotating collapsed object. James Bardeen has recently emphasized that all stars have angular momentum and that most stars—or star cores—will have so much angular momentum that the black hole formed upon collapse will be rotating at the



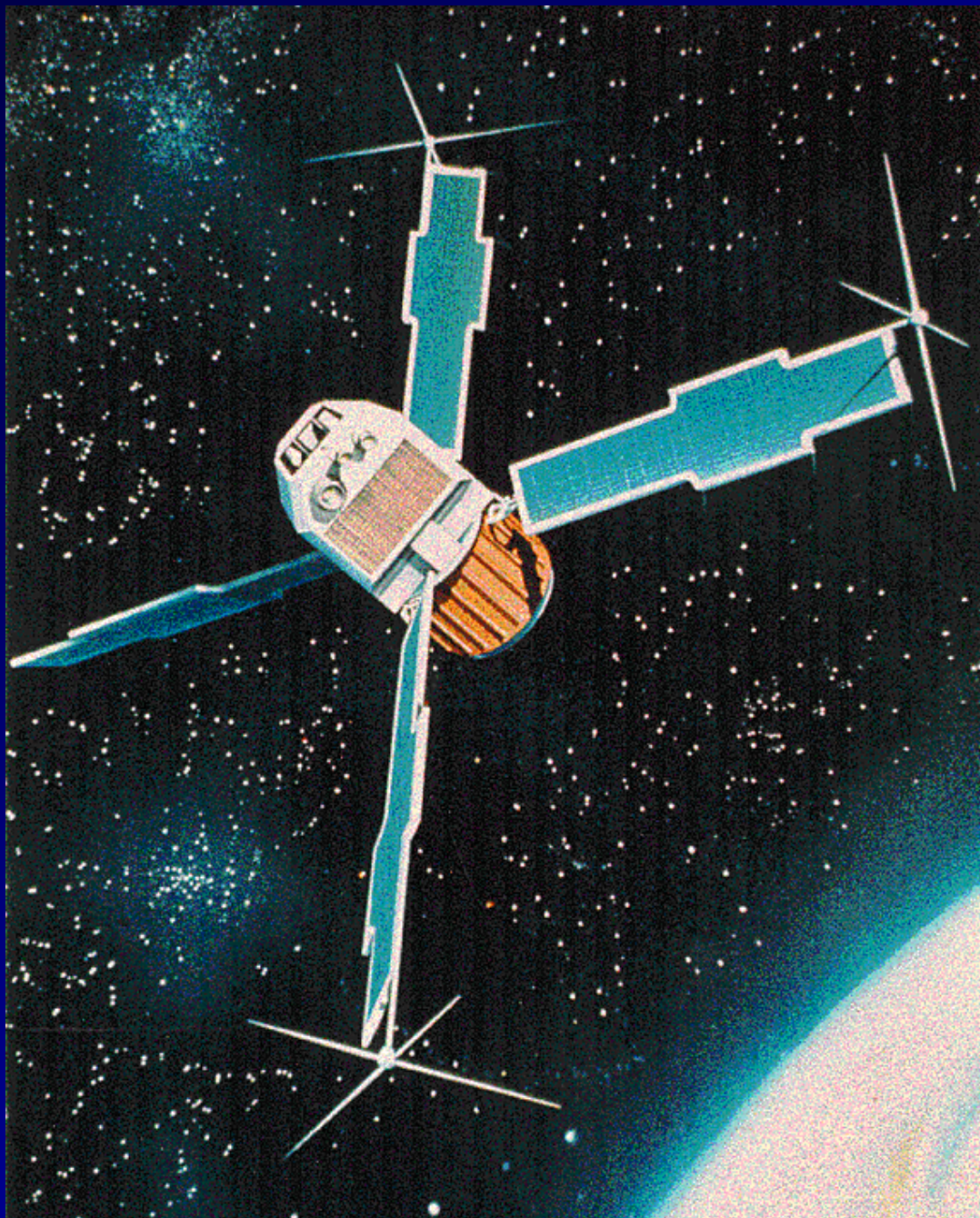
Remo Ruffini and John Wheeler are both at Princeton University; Wheeler, currently on leave from Princeton, is spending a year at Cal Tech and Moscow State University.



Uhuru satellite (1970-1973) Uhuru

X-Ray: 2-20 keV

The satellite Uhuru was launched from an Italian platform from Kenya, the days of independence of Kenya: Uhuru means freedom in SWAHILI



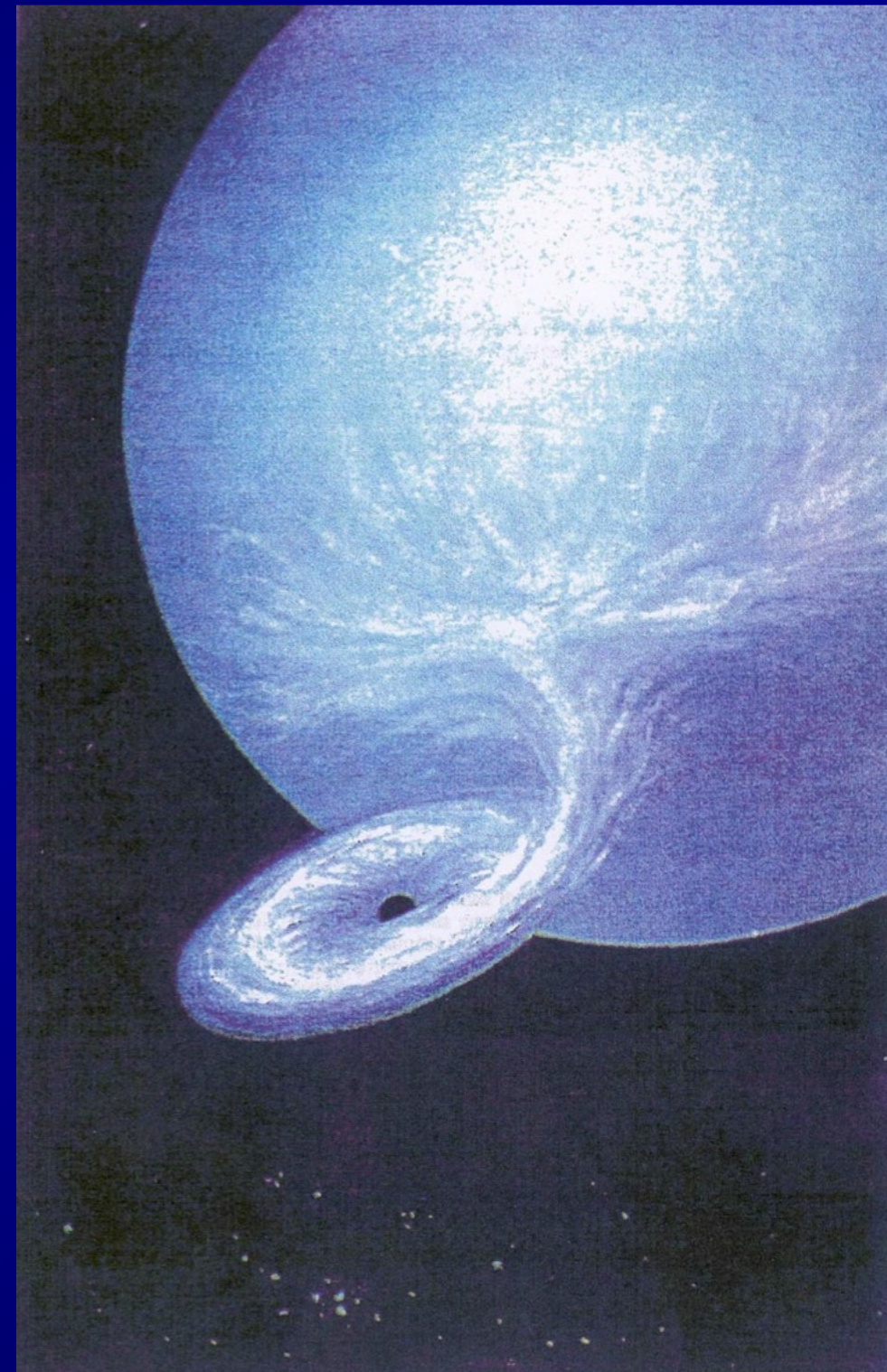
The identification of the first black hole in our galaxy: Cygnus X-1

$$\text{Luminosity} = 10^{37} \text{ erg/s} = 10^4 L_\odot \\ = 0.01(dm/dt)_{\text{acc}} c^2$$

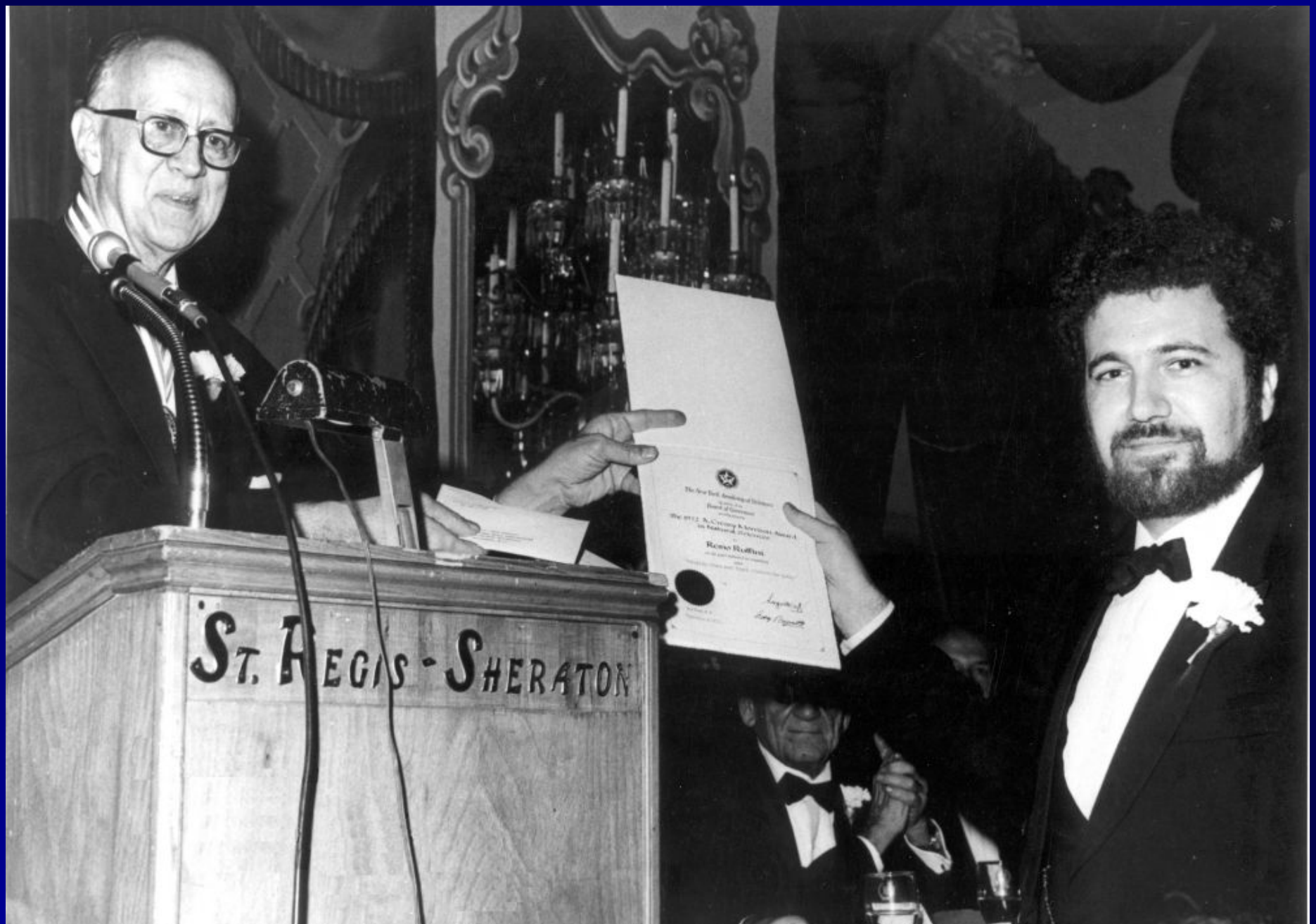
Absence of pulsation due to uniqueness of Kerr-Newmann black holes

$$M > 3.2 M_\odot$$

Leach & Ruffini, 1973



Cressy – Morrison award (NY, 1973, Cressy – Morrison)

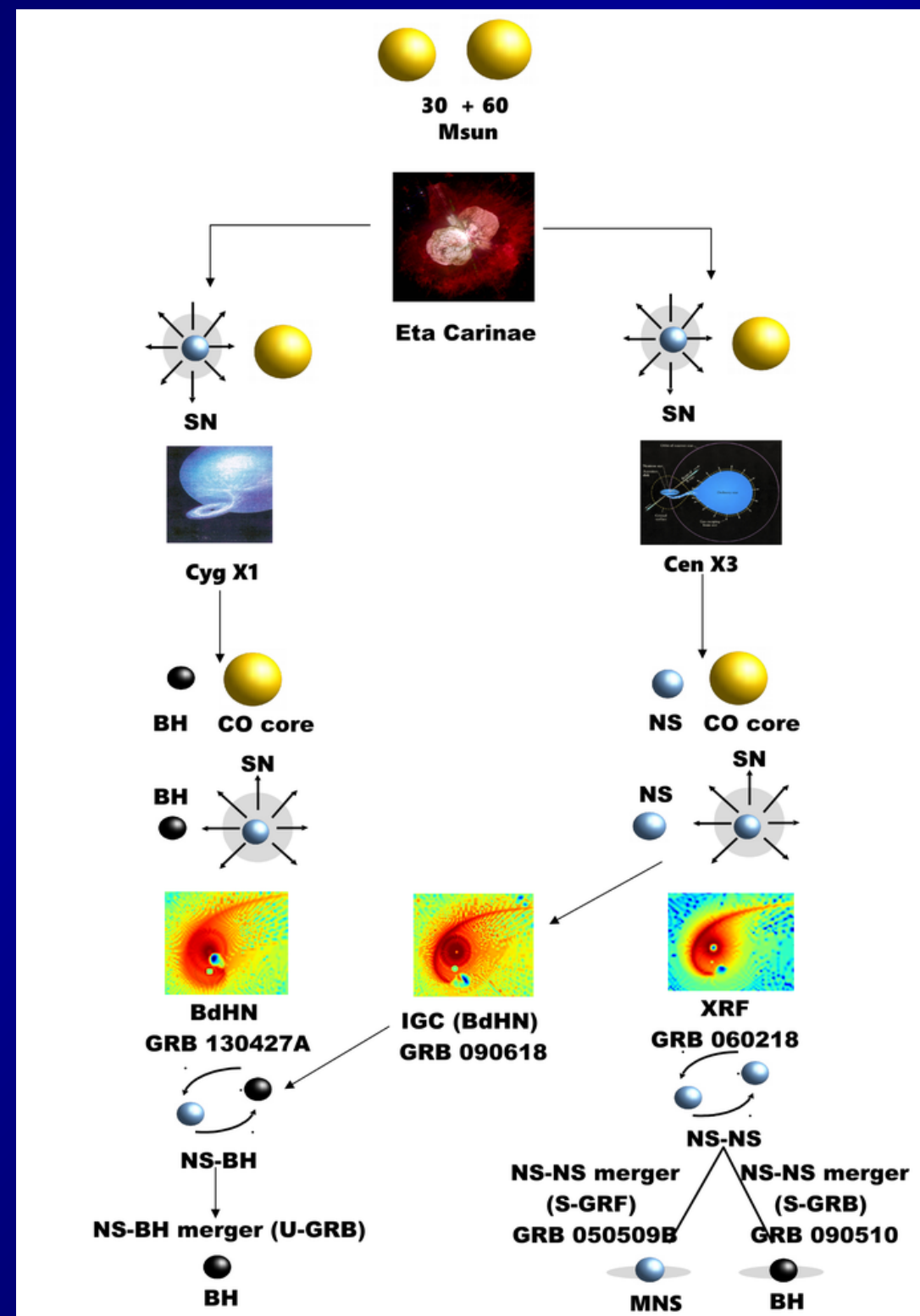


Giacconi, Sweden (2002)



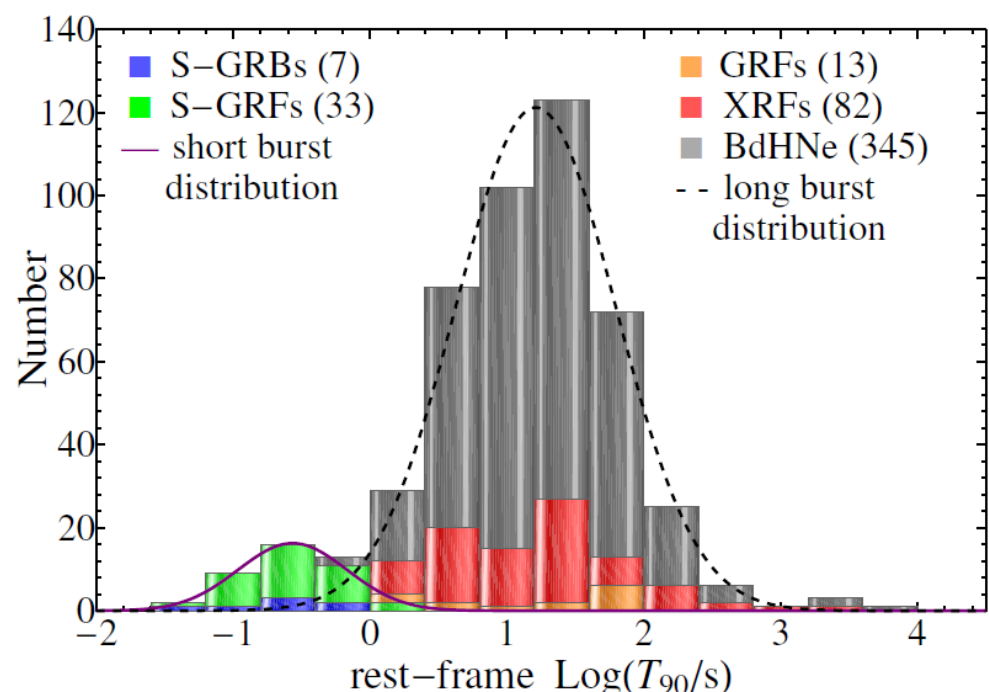
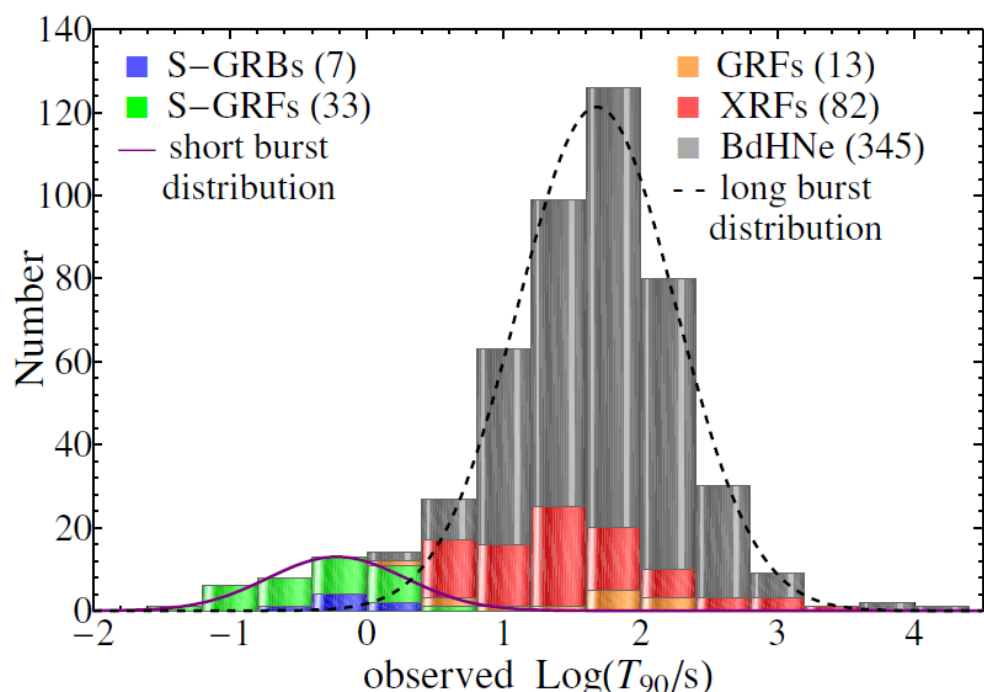
A common evolutionary scenario for short and long GRBs

Rueda, Ruffini, *ApJL*, **758** (2012) L7
 Becerra, Cipolletta, Fryer, Rueda, Ruffini, *ApJ*, **812** (2015) 100
 Fryer, Oliveira, Rueda, Ruffini, *Phys. Rev. Lett.*, **115** (2015) 23
 Ruffini, Rueda, et al., *ApJ*, **832** (2016) 136

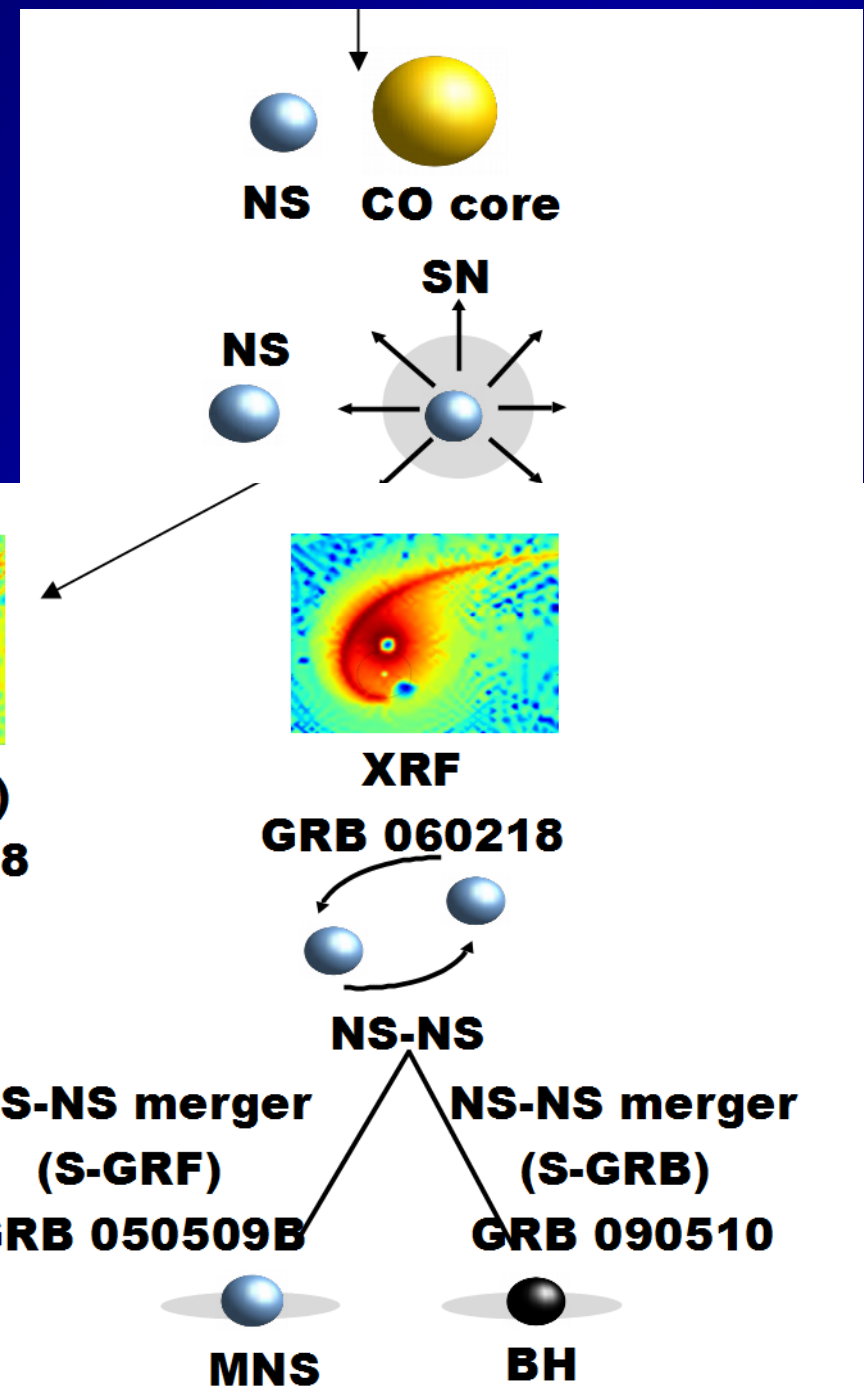


Eight different GRB families

	Sub-class	Number	In-state	Out-state	$E_{p,i}$ (MeV)	E_{iso} (erg)	$E_{iso, GeV}$ (erg)
I	S-GRFs	17	NS-NS	MNS	$\sim 0.2\text{--}2$	$\sim 10^{49}\text{--}10^{52}$	—
II	S-GRBs	6	NS-NS	BH	$\sim 2\text{--}8$	$\sim 10^{52}\text{--}10^{53}$	$\gtrsim 10^{52}$
III	XRFs	48	CO _{core} -NS	ν NS-NS	$\sim 0.004\text{--}0.2$	$\sim 10^{48}\text{--}10^{52}$	—
IV	BdHNe	329	CO _{core} -NS	ν NS-BH	$\sim 0.2\text{--}2$	$\sim 10^{52}\text{--}10^{54}$	$\gtrsim 10^{52}$
V	BH-SN	4	CO _{core} -BH	ν NS-BH	$\gtrsim 2$	$> 10^{54}$	$\gtrsim 10^{53}$
VI	U-GRBs	0	ν NS-BH	BH	$\gtrsim 2$	$> 10^{52}$	—
VII	GRFs	1	NS-WD	MNS	$\sim 0.2\text{--}2$	$\sim 10^{51}\text{--}10^{52}$	—
VIII	GR-K	1	WD-WD	MWD	~ 0.082	$\sim 10^{47}$	—



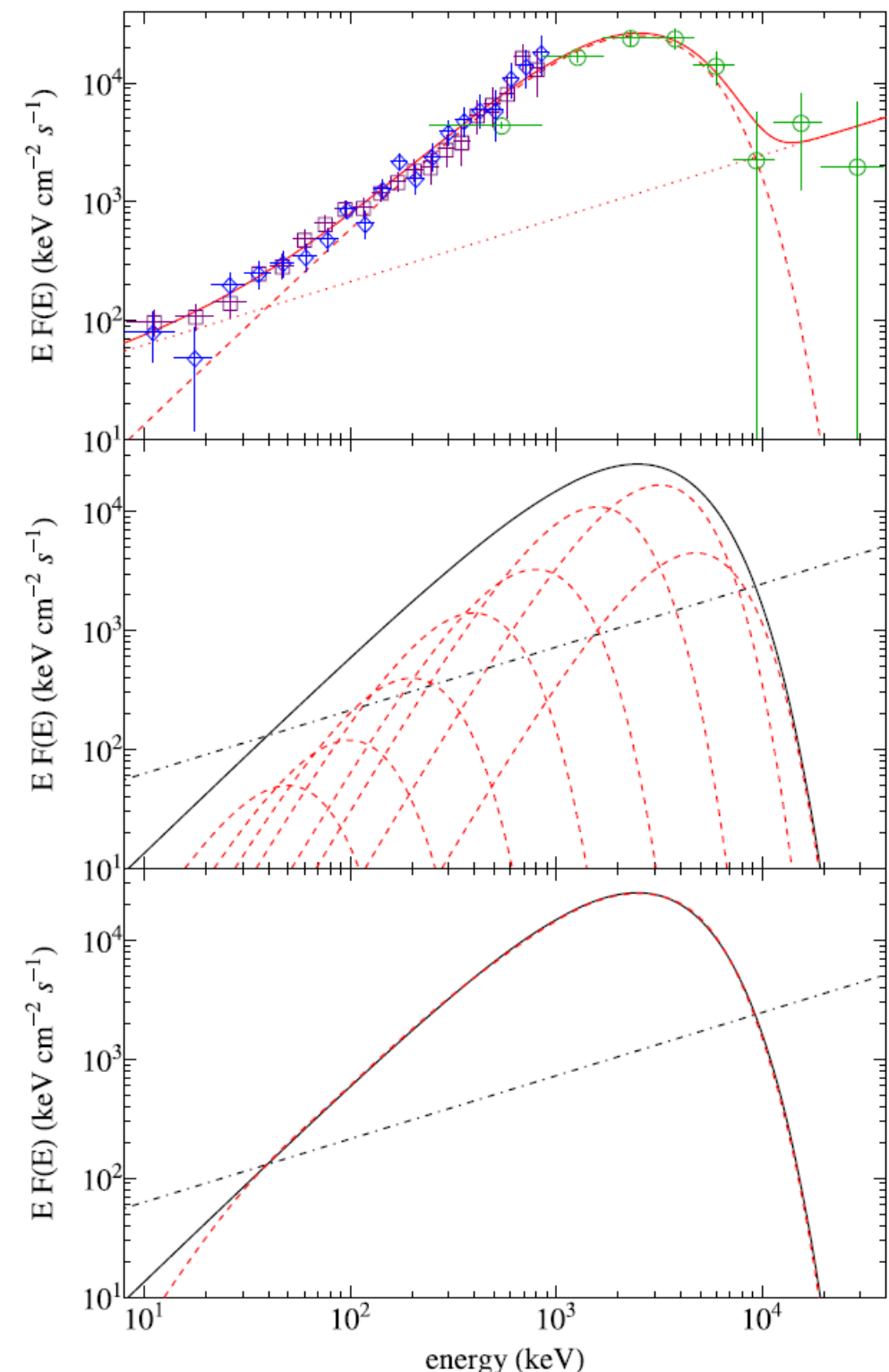
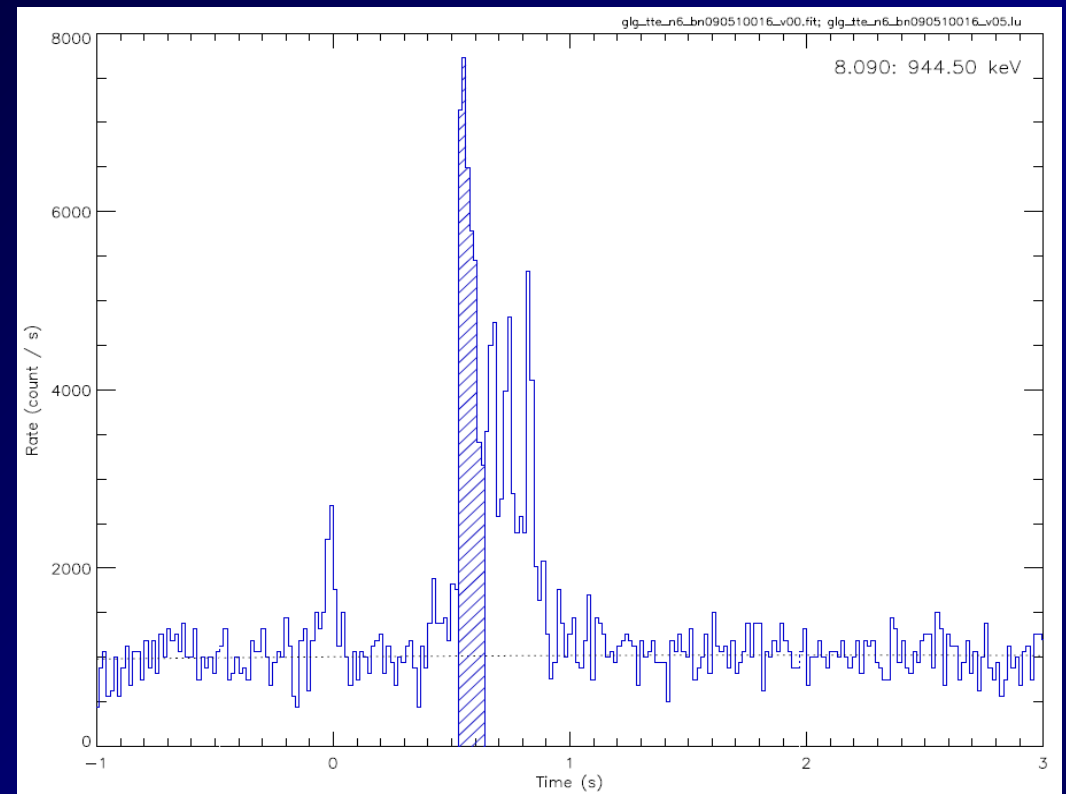
The Binary-Driven Hypernovae (BdHNe)



No GeV Emission in Short GRFs

Group	S-GRF	z	E_p keV	E_{iso} (10^{50} erg)	Fermi GCN	θ (deg)	GeV observed	Comments
	090426	2.609		44.5 ± 6.6	—	—	no	Upgraded to S-GRB at MG15
No <i>Fermi</i> Observation	090515	0.403		0.094 ± 0.014	—	—	no	
	100724A	1.288		16.4 ± 2.4	—	—	no	
	101219A	0.718		48.8 ± 6.8	—	—	no	
	120804A	1.3		70.0 ± 15.0	—	—	no	46^{day} x-ray (GCN 13841)
	130603B	0.356		21.2 ± 2.3	—	—	no	kilonova (GCN 14893, 14895, 14913)
	140622A	0.959		0.70 ± 0.13	—	—	no	
	140903A	0.351		1.41 ± 0.11	—	—	no	
	090927	1.37	408.64	7.6 ± 3.5	GCN 9974	85.0	no	
Outside Boresight Angle	100117A	0.915	625.73	78.0 ± 10.0	GCN 10345	86.0	no	
	100625A	0.453	701.81	7.50 ± 0.30	GCN 10912	125.0	no	
	131004A	0.717	202.45	12.7 ± 0.9	GCN 15315	93.0	no	
	141004A	0.573	268.99	21.0 ± 1.9	GCN 16900	100.4	no	
	080905A	0.122	443.12	6.58 ± 0.96	GCN 8204	28.0	no	
Inside Boresight Angle	100206A	0.408	748.34	4.67 ± 0.61	GCN 10381	44.7	no	
	111117A	1.31	857.40	34.0 ± 13.0	GCN 12573	12.0	no	
	150101B	0.134	141.88	0.4	GCN 17276	44.0	no	, 39^{day} x-ray (GCN 17431)
	160821B	0.16	97.44	1.2	GCN 19843	61.0	no	kilonova

GRB 090510: P-GRB Light Curve and Spectrum

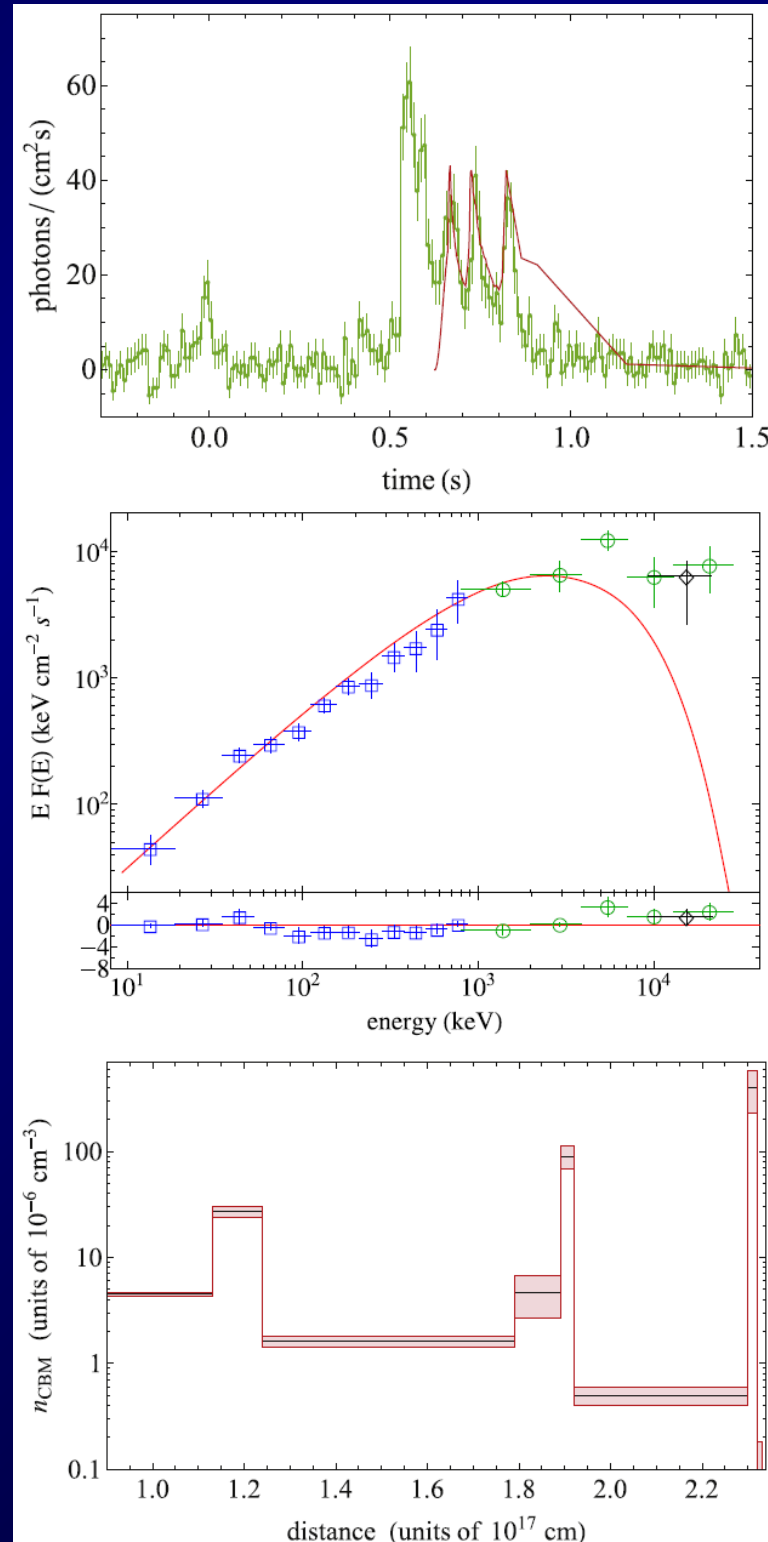


GRB 090510: Prompt emission Light Curve and Spectrum

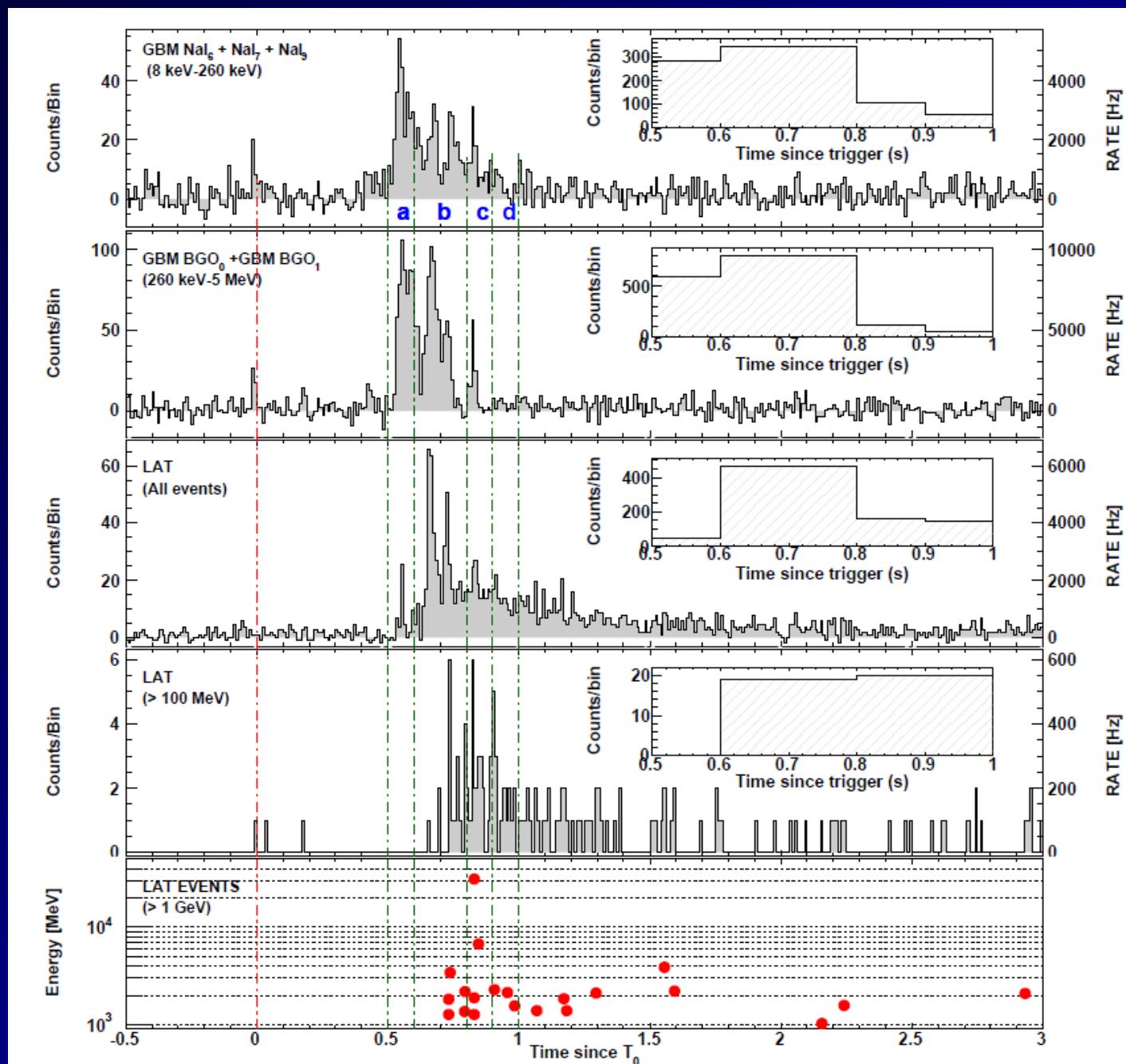
$z_{\text{obs}} = 0.903 \pm 0.003$ (spectroscopic

determination from the host
galaxy located by VLT/FORS2)

$z_{\text{th}} = 0.75 \pm 0.17$ (theoretically
determined from the Fireshell
theory)



GRB 090510



Spectra and GeV emission in S-GRBs

Source	z	$E_{\text{p,i}}$ (MeV)	E_{iso} (10^{52} erg)	Fermi GCN	E_{LAT} (10^{52} erg)	θ (deg)	TS	comments
081024B	3.12	9.56 ± 4.94	2.64 ± 1.00	8407, 8408	$\gtrsim 2.79 \pm 0.98$	18.7	111	
090426	2.609		44.5 ± 6.6	–	–	-	-	No <i>Fermi</i> observation
090510A	0.903	7.89 ± 0.76	3.95 ± 0.21	9334, 9336	$\gtrsim 5.78 \pm 0.60$	13.6	1897	possible kilonova
140402A	5.52	6.1 ± 1.6	4.7 ± 1.1	16069, 16070	$\gtrsim 4.5 \pm 2.2$	13	45	
140619B	2.67	5.34 ± 0.79	6.03 ± 0.79	16419, 16420	$\gtrsim 2.34 \pm 0.91$	32	149	
160829A	4.373	0.92 ± 0.34	2.56 ± 0.22	19879	$\gtrsim 3.39 \pm 2.95$	14.8	30.5	

Rest-frame GeV luminosity in S- GRBs

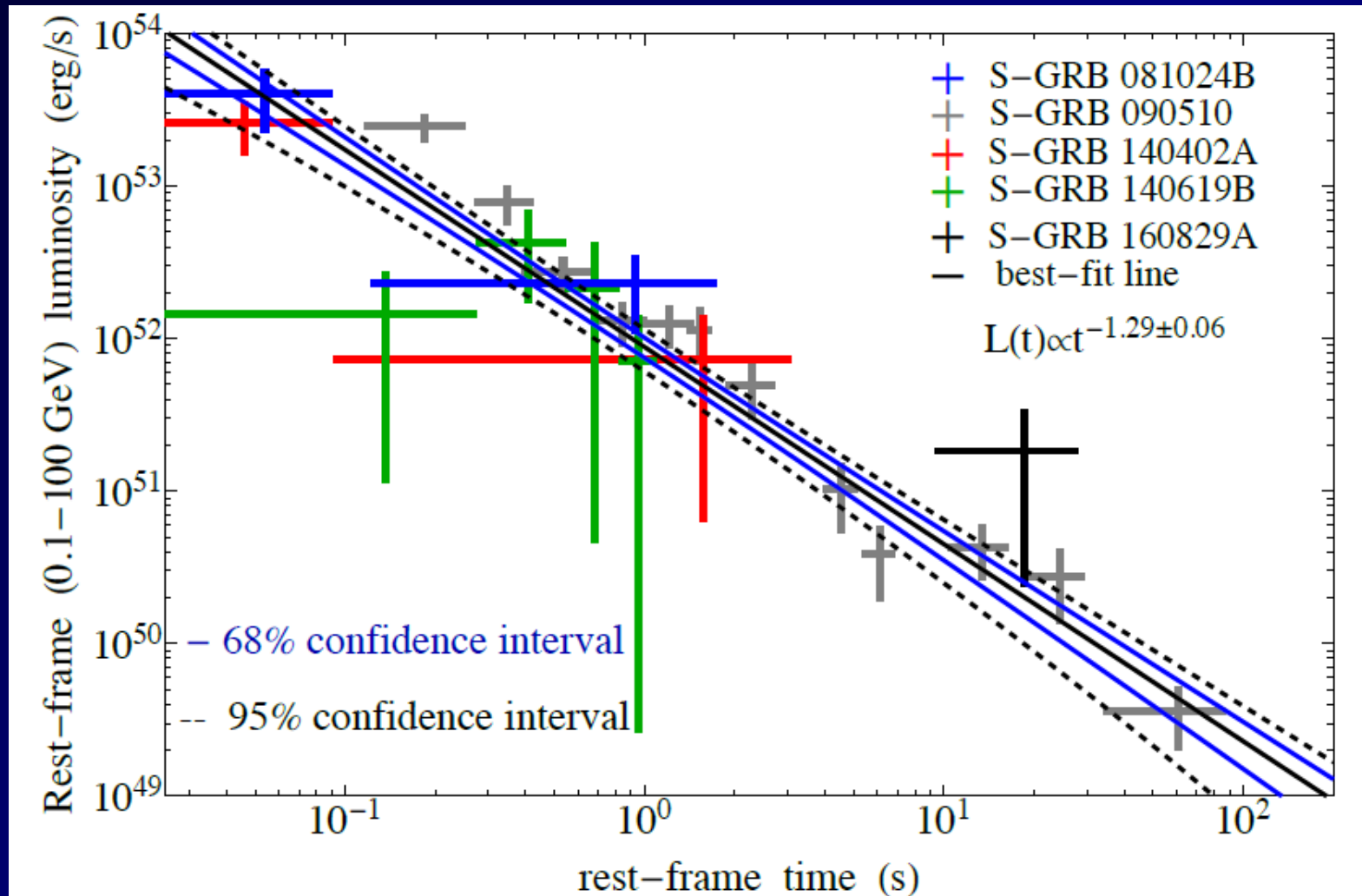
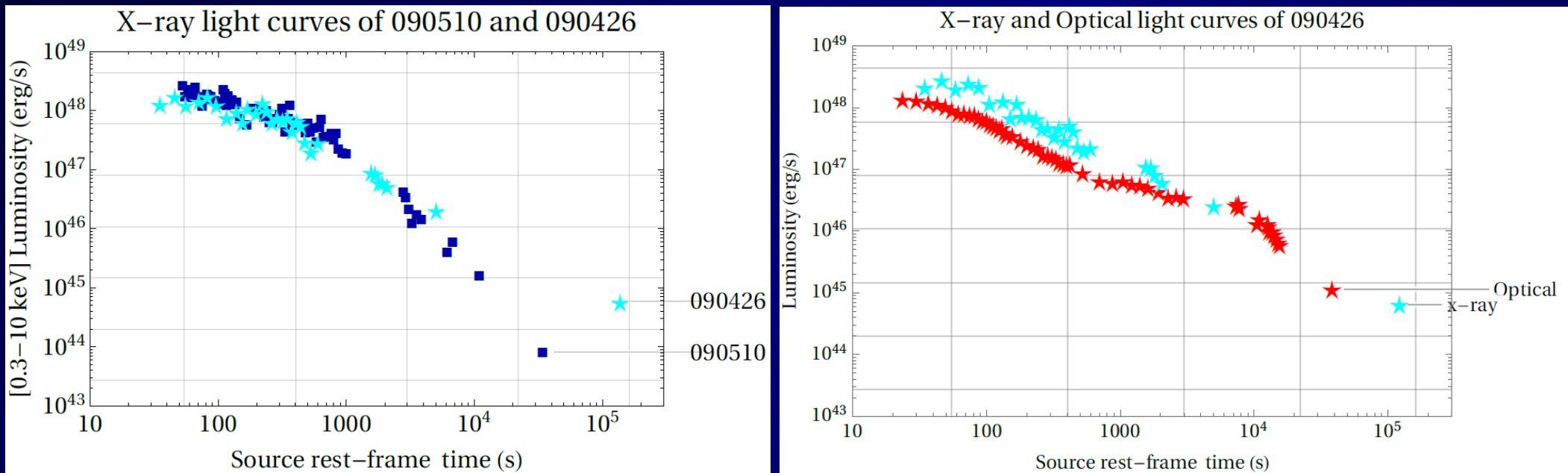


Figure 2. The rest-frame 0.1–100 GeV isotropic luminosity light-curves of all S-GRBs with LAT emission. The black line indicate the common power-law behavior of the GeV emission with the slope of $\gamma = -1.29 \pm 0.06$.

Complementarity of S-GRBs 090510, 090426 and 140619B



090510 (Fermi, Agile and Swift)
090426 (No Fermi data and $z_{\text{obs}} = 2.609$ – No GeV)
140619B (Fermi and derived $z_{\text{th}} = 0.9$ independent on GeV observation)



Remo Ruffini and Roy Kerr at Stephen Hawking's home on July 2017





The Black Hole Mass-Energy Formula

$$m^2 = \left(m_{ir} + \frac{e^2}{4m_{ir}} \right)^2 + \frac{L^2}{4m_{ir}^2}$$

$$S = 16\pi m_{ir}^2$$

$$\delta S = 32\pi m_{ir} \delta m_{ir} \geq 0$$

Christodoulou, *Phys. Rev. Lett.*, **25** (1970) 1596 (received September 17th, 1970)
Christodoulou, Ruffini, *Phys. Rev. D*, **4** (1971) 3552 (received March 1st, 1971)
Hawking, *Phys. Rev. Lett.*, **26** (1971) 1344 (received March 11th, 1971)
Hawking, *Commun. Math. Phys.*, **25** (1972) 152 (received October 15th, 1971)

NS critical mass vs. spin parameter

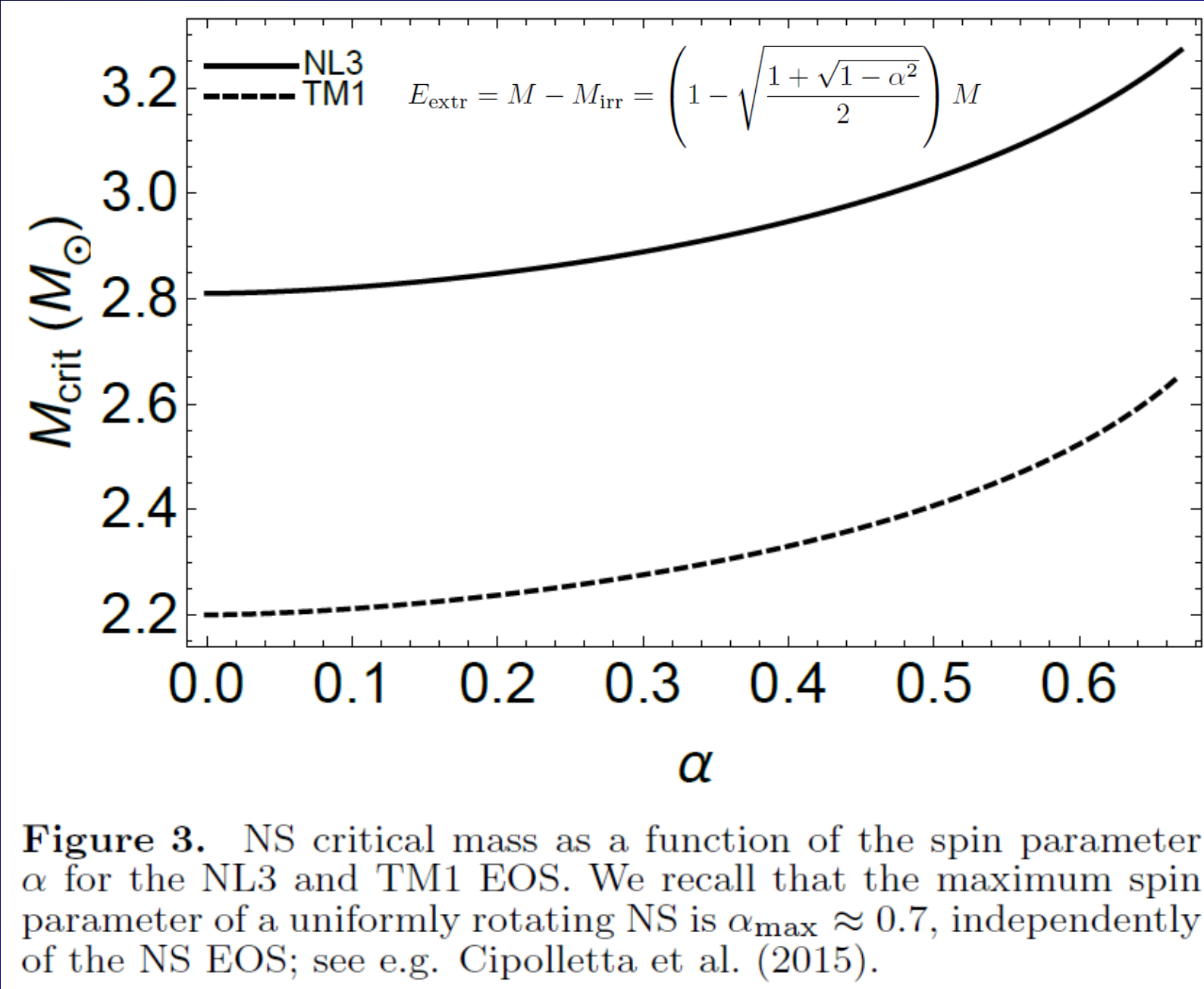


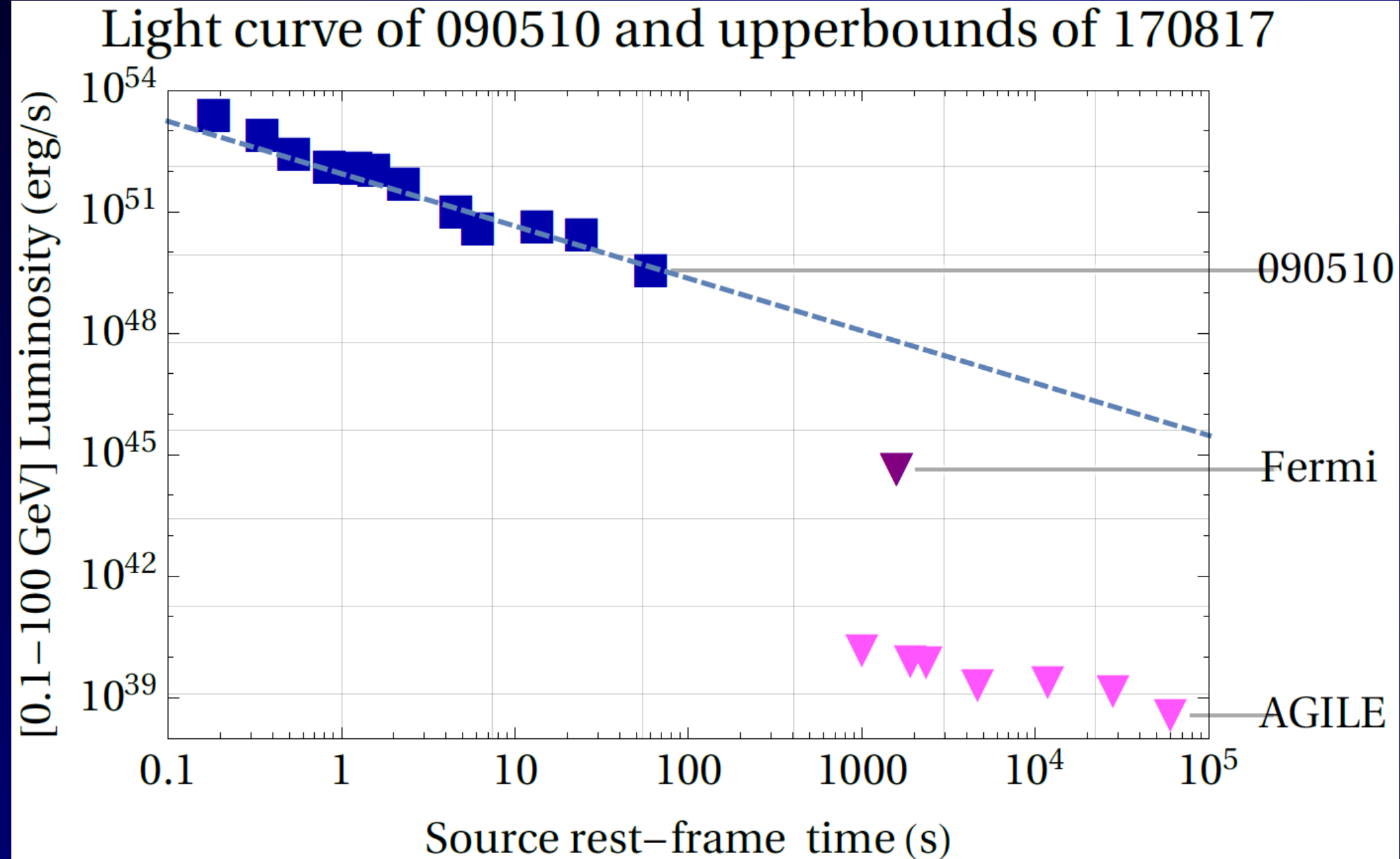
Figure 3. NS critical mass as a function of the spin parameter α for the NL3 and TM1 EOS. We recall that the maximum spin parameter of a uniformly rotating NS is $\alpha_{\text{max}} \approx 0.7$, independently of the NS EOS; see e.g. Cipolletta et al. (2015).

The spin and the mass of the Kerr BH in short GRBs

Source	TM1		NL3	
	α	$M(\alpha)$ (M _⊕)	α	$M(\alpha)$ (M _⊕)
S-GRB 081024B	$0.23^{+0.04}_{-0.04}$	$2.25^{+0.01}_{-0.01}$	$0.21^{+0.03}_{-0.04}$	$2.85^{+0.01}_{-0.01}$
S-GRB 090426	—	—	—	—
S-GRB 090510A	$0.33^{+0.02}_{-0.02}$	$2.29^{+0.01}_{-0.01}$	$0.30^{+0.01}_{-0.01}$	$2.89^{+0.01}_{-0.01}$
S-GRB 140402A	$0.29^{+0.06}_{-0.08}$	$2.27^{+0.03}_{-0.03}$	$0.26^{+0.05}_{-0.07}$	$2.87^{+0.03}_{-0.03}$
S-GRB 140619B	$0.21^{+0.04}_{-0.05}$	$2.24^{+0.01}_{-0.02}$	$0.19^{+0.04}_{-0.05}$	$2.85^{+0.01}_{-0.01}$
S-GRB 160829A	$0.29^{+0.10}_{-0.18}$	$2.27^{+0.05}_{-0.06}$	$0.26^{+0.09}_{-0.17}$	$2.87^{+0.04}_{-0.05}$

The short GRB contribution to understanding the nature of GRB 170817: no BH

Light curve of 090510 and upperbounds of 170817



Short GRBs

- Contrary to all the other GRB families, short GRBs (S-GRBs) all have comparable mass-energies.
- Their GeV luminosity, in the source rest frame, overlap and follows a universal power law behavior.
- The redshift is observed, z_{obs} , only in two cases (GRB 090510, GRB 090426), in all other S-GRBs it has been theoretically determined, z_{th} . The GeV emission is not used in determining the z_{th} , therefore the overlapping of the GeV emission

The BdHN basic structure

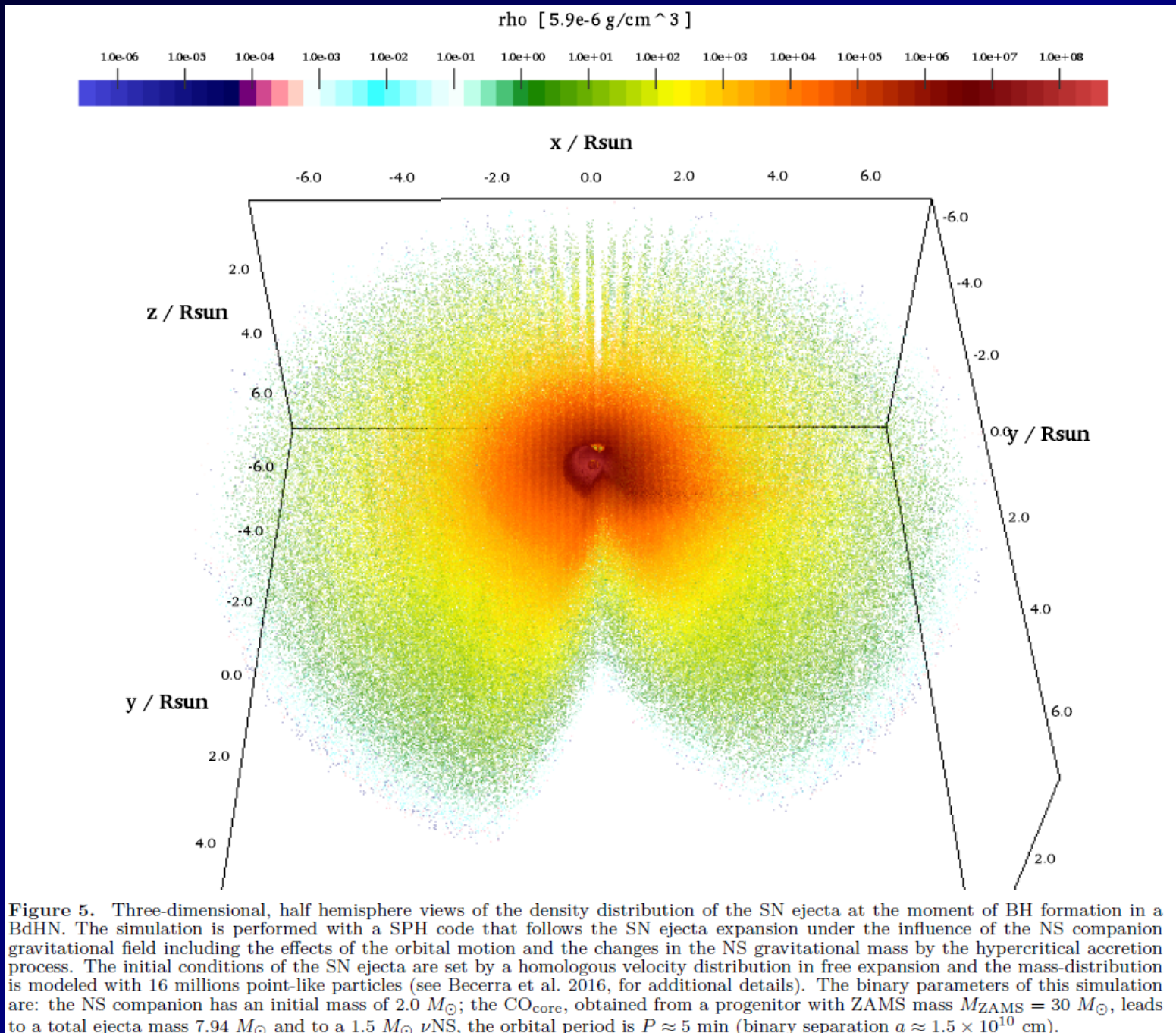
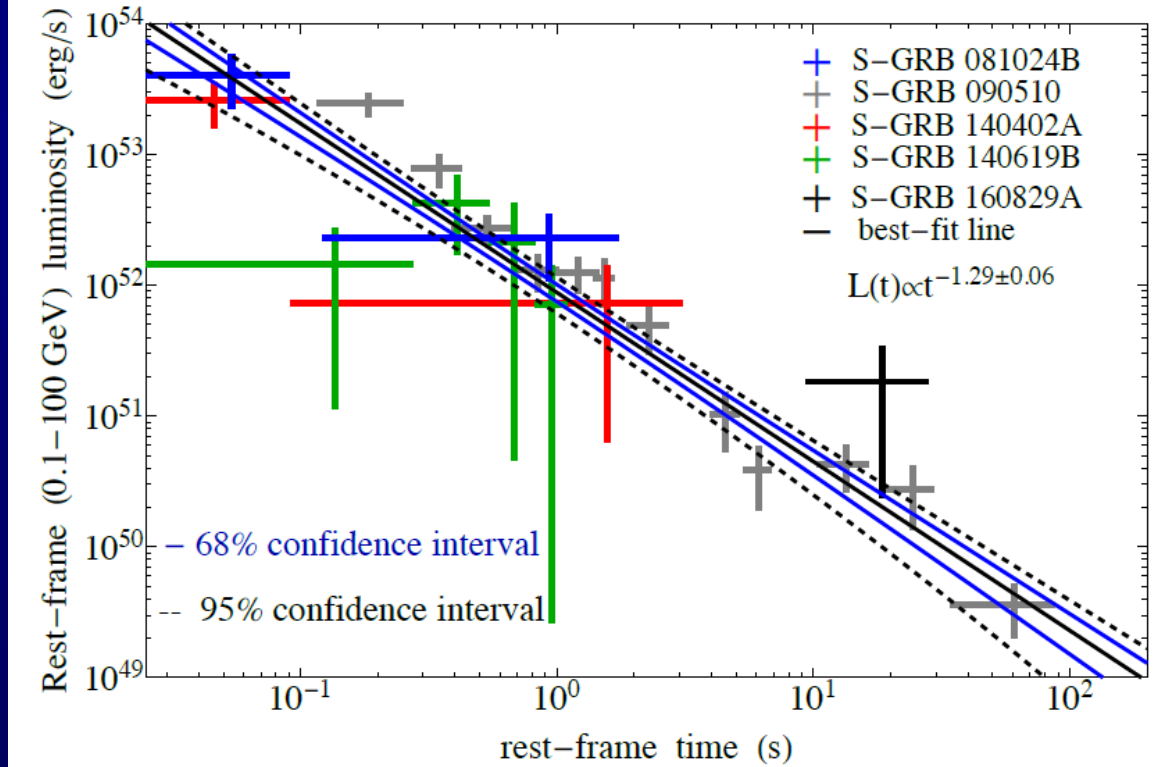
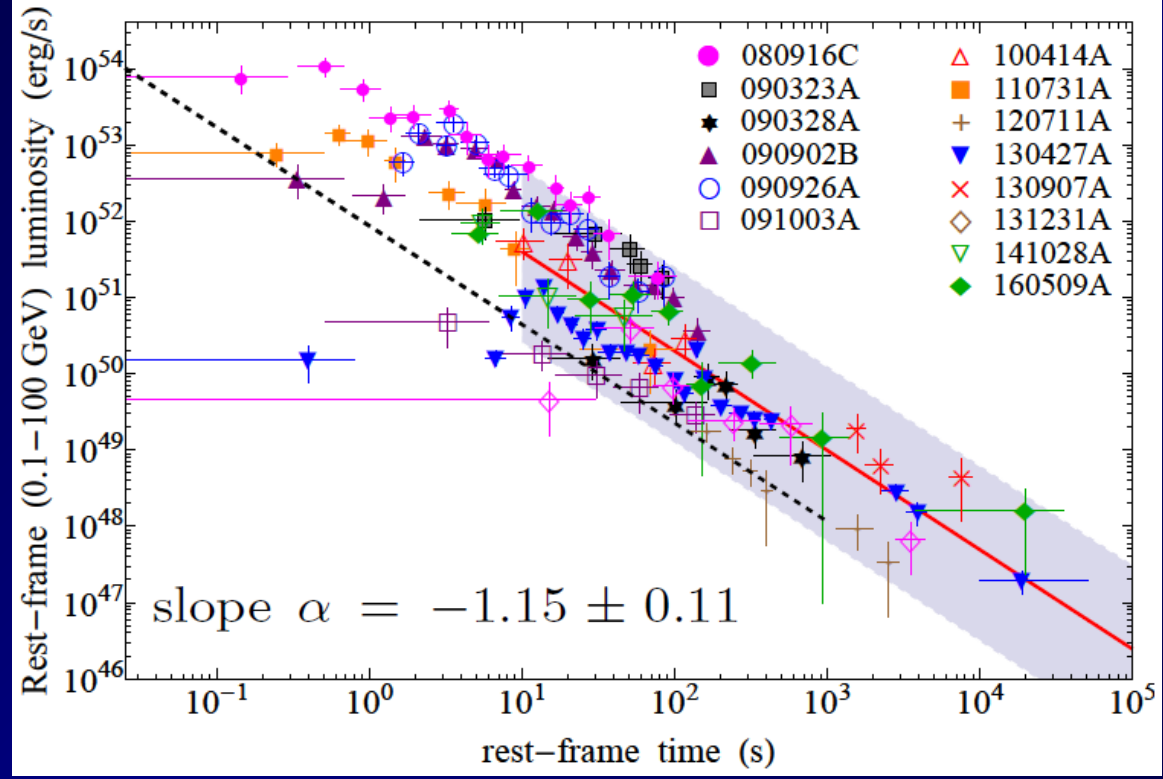


Figure 5. Three-dimensional, half hemisphere views of the density distribution of the SN ejecta at the moment of BH formation in a BdHN. The simulation is performed with a SPH code that follows the SN ejecta expansion under the influence of the NS companion gravitational field including the effects of the orbital motion and the changes in the NS gravitational mass by the hypercritical accretion process. The initial conditions of the SN ejecta are set by a homologous velocity distribution in free expansion and the mass-distribution is modeled with 16 millions point-like particles (see Becerra et al. 2016, for additional details). The binary parameters of this simulation are: the NS companion has an initial mass of $2.0 M_{\odot}$; the CO_{core}, obtained from a progenitor with ZAMS mass $M_{ZAMS} = 30 M_{\odot}$, leads to a total ejecta mass $7.94 M_{\odot}$ and to a $1.5 M_{\odot}$ νNS, the orbital period is $P \approx 5$ min (binary separation $a \approx 1.5 \times 10^{10}$ cm).

GeV emission in BdHNe and in S-GRBs

Ruffini, Rueda, et al., *ApJ*, 832 (2016) 136
 Aimuratov, Ruffini, et al., *ApJ*, in press, arXiv:1704.08179
 Ruffini, et al. arXiv:1802.07552
 Ruffini, et al. arXiv:1803.05476



BdHNe without GeV Emission

BdHNe	z	E_p keV	E_{iso} (10^{52} erg)	Fermi GCN	θ (deg)	GeV observed	comments
081118	2.58		12.2 ± 1.2	GCN 8550	41.0	no	
081222	2.77		27.4 ± 2.7	GCN 8715	50.0	no	
090424A	0.544		4.07 ± 0.41	GCN 9230	71.0	no	
090516A	4.109	948.23 ± 359.93	99.6 ± 16.7	GCN 9415	20.0	no	Clear X-ray flare observed
091127A	0.49		1.64 ± 0.18	GCN 10204	25.0	no	
100615A	1.398		5.81 ± 0.11	GCN 10851	64.0	no	
100728B	2.106		3.55 ± 0.36	GCN 11015	57.1	no	
110128A	2.339		1.58 ± 0.21	GCN 11628	45.0	no	
111228A	0.716		2.75 ± 0.28	GCN 12744	70.0	no	
120119A	1.728		27.2 ± 3.6	GCN 12874	31.4	no	
120712A	4.175		21.2 ± 2.1	GCN 13469	42.0	no	
120716A	2.486		30.2 ± 3.0	GCN 13498	63.0	no	
120909A	3.93		87 ± 10	GCN 13737	66.0	no	
130528A	1.250	266.18 ± 179.33	18.01 ± 2.28	GCN 14729	60.0	no	X-ray flare observed
130925A	0.347	144.13 ± 4.04	3.23 ± 0.37	GCN 15261	22.0	no	X-ray flare observed
131105A	1.686		34.7 ± 1.2	GCN 15455	37.0	no	
*140206A	2.73	1106.32 ± 27.23	144.24 ± 19.20	GCN 15790	46.0	no(?)	(To Verify,15791),Clear X-ray flare observed
140213A	1.2076		9.93 ± 0.15	GCN 15833	48.5	no	
140423A	3.26		65.3 ± 3.3	GCN 16152	44.0	no	
141623A	1.92		7.69 ± 0.68	GCN 16450	32.0	no	
140703A	4.13		1.72 ± 0.09	GCN 16512	16.0	no	
140907A	1.21	249.73 ± 15.47	2.29 ± 0.08	GCN 16798	16.0	no	X-ray flare observed
141220A	1.3195		2.44 ± 0.07	GCN 17205	47.0	no	
150301B	1.5169		2.87 ± 0.42	GCN 17525	39.0	no	
150821A	0.755		14.7 ± 1.1	GCN 18190	57.0	no	
151027A	0.81	615.40 ± 114.03	3.94 ± 1.33	GCN 18492	10.0	no	Clear X-ray flare observed
151111A	3.5	254.70 ± 41.41	3.43 ± 1.19	GCN 18582	50.0	no	X-ray flare observed
161014A	2.823		10.1 ± 1.7	GCN 20051	69.0	no	

Table 10

List of 25 (updated 28) BdHNe inside Fermi-LAT boresight angle and no GeV photon detected: 25 (updated 28) BdHNe with redshift taken from (Ruffini et al. 2016b) from 2008, when Fermi started to operate, till the end of 2016. All of them are within the boresight of Fermi-LAT, but none detected GeV photon. For each source the columns list: z , E_{iso} , E_p , GCN number, position of the source from LAT boresight θ , whether was detection by LAT, and additional information.

BdHNe with GeV Emission

BdHNe	A_n (Amplitude)	uncertainty of A_n	α (Index)	uncertainty of α	L_{10s}	error of L_{10s}
080916C	4.396×10^{53}	$\pm 1.34 \times 10^{53}$	1.15	± 0.11	3.255×10^{52}	$+1.152 -1.003 \times 10^{52}$
090323	3.008×10^{53}	$\pm 9.84 \times 10^{52}$	1.15	± 0.11	2.227×10^{52}	$+8.301 -7.222 \times 10^{51}$
090328	1.187×10^{53}	$\pm 4.52 \times 10^{51}$	1.15	± 0.11	8.791×10^{50}	$+3.872 -3.177 \times 10^{50}$
090902B	1.716×10^{53}	$\pm 3.68 \times 10^{52}$	1.15	± 0.11	1.270×10^{52}	$+3.425 -2.847 \times 10^{51}$
090926A	1.99×10^{53}	$\pm 4.75 \times 10^{52}$	1.15	± 0.11	1.472×10^{52}	$+4.222 -3.680 \times 10^{51}$
091003A	4.551×10^{51}	$\pm 1.64 \times 10^{51}$	1.15	± 0.11	3.369×10^{50}	$+1.319 -1.214 \times 10^{50}$
100414A	2.681×10^{52}	$\pm 1.23 \times 10^{52}$	1.15	± 0.11	1.985×10^{51}	$+1.015 -0.896 \times 10^{51}$
110731A	4.579×10^{52}	$\pm 2.09 \times 10^{52}$	1.15	± 0.11	3.390×10^{51}	$+1.707 -1.563 \times 10^{51}$
120711A	3.776×10^{51}	$\pm 1.26 \times 10^{51}$	1.15	± 0.11	2.796×10^{50}	$+1.162 -0.882 \times 10^{50}$
130427A	1.575×10^{52}	$\pm 3.07 \times 10^{51}$	1.15	± 0.11	1.166×10^{51}	$+2.803 -2.309 \times 10^{50}$
130907A	5.209×10^{52}	$\pm 3.09 \times 10^{52}$	1.15	± 0.11	3.857×10^{51}	$+2.770 -2.092 \times 10^{51}$
131231A	1.520×10^{51}	$\pm 9.02 \times 10^{50}$	1.15	± 0.11	1.125×10^{50}	$+6.895 -6.678 \times 10^{49}$
141028A	3.185×10^{52}	$\pm 1.64 \times 10^{52}$	1.15	± 0.11	2.358×10^{51}	$+1.282 -1.219 \times 10^{51}$
160509A	5.829×10^{52}	$\pm 1.24 \times 10^{52}$	1.15	± 0.11	4.316×10^{51}	$+1.073 -0.967 \times 10^{51}$

Table 7

Fitting results of BdHNe with GeV emission in Tab. 6: a list including the amplitude of BdHN (A_n) and its uncertainty, the common power-law index α and its uncertainty. The inferred luminosity of 0.1–100 GeV at 10 s from the fitting and its uncertainty.

The spin and the mass of the Kerr BH in BdHNe

Source	TM1		NL3	
	α	$M(\alpha)$ (M_\odot)	α	$M(\alpha)$ (M_\odot)
BdHN 090328A	$0.2434^{+0.0004}_{-0.0004}$	$2.2526^{+0.0001}_{-0.0001}$	$0.2167^{+0.0003}_{-0.0003}$	$2.8538^{+0.0001}_{-0.0001}$
BdHN 091003A	$0.161^{+0.002}_{-0.002}$	$2.2259^{+0.0005}_{-0.0005}$	$0.143^{+0.001}_{-0.001}$	$2.8311^{+0.0004}_{-0.0004}$
BdHN 100414A	$0.400^{+0.006}_{-0.006}$	$2.330^{+0.004}_{-0.004}$	$0.359^{+0.006}_{-0.006}$	$2.921^{+0.003}_{-0.003}$
BdHN 110731A	$0.68^{+0.05}_{-0.06}$	$2.57^{+0.12}_{-0.10}$	$0.62^{+0.05}_{-0.06}$	$3.18^{+0.09}_{-0.09}$
BdHN 120711A	$0.08160^{+0.00008}_{-0.00008}$	$2.20849^{+0.00001}_{-0.00001}$	$0.07227^{+0.00007}_{-0.00007}$	$2.81662^{+0.00001}_{-0.00001}$
BdHN 130427A	$0.327^{+0.001}_{-0.001}$	$2.2893^{+0.0006}_{-0.0006}$	$0.293^{+0.001}_{-0.001}$	$2.8854^{+0.0005}_{-0.0005}$
BdHN 130907A	$0.22560^{+0.00005}_{-0.00005}$	$2.24606^{+0.00002}_{-0.00002}$	$0.20068^{+0.00004}_{-0.00004}$	$2.84823^{+0.00001}_{-0.00001}$
BdHN 131231A	$0.2075^{+0.0007}_{-0.0007}$	$2.2399^{+0.0002}_{-0.0002}$	$0.1844^{+0.0006}_{-0.0006}$	$2.8430^{+0.0002}_{-0.0002}$
BdHN 141028A	$0.37^{+0.01}_{-0.01}$	$2.312^{+0.006}_{-0.006}$	$0.331^{+0.009}_{-0.010}$	$2.905^{+0.005}_{-0.005}$
BdHN 160509A	$0.707^{+0.002}_{-0.002}$	$2.636^{+0.004}_{-0.004}$	$0.651^{+0.002}_{-0.002}$	$3.232^{+0.003}_{-0.003}$

Table 8

The BH spin parameter α and mass M within the TM1 and the NL3 nuclear models, as inferred from the values of E_{LAT} for 10 BdHNe, out of the 14 ones in Fig. 3, providing BH spin parameters $\alpha < 0.71$.

The topology of the BdHN supernova ejecta

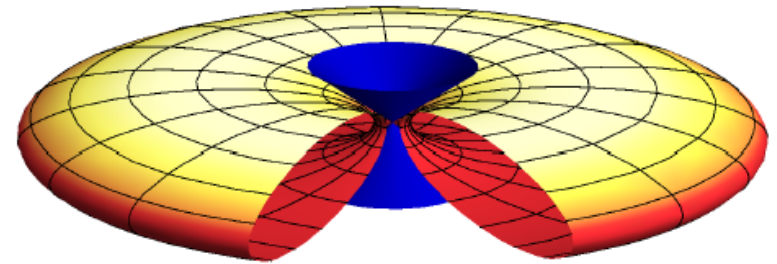
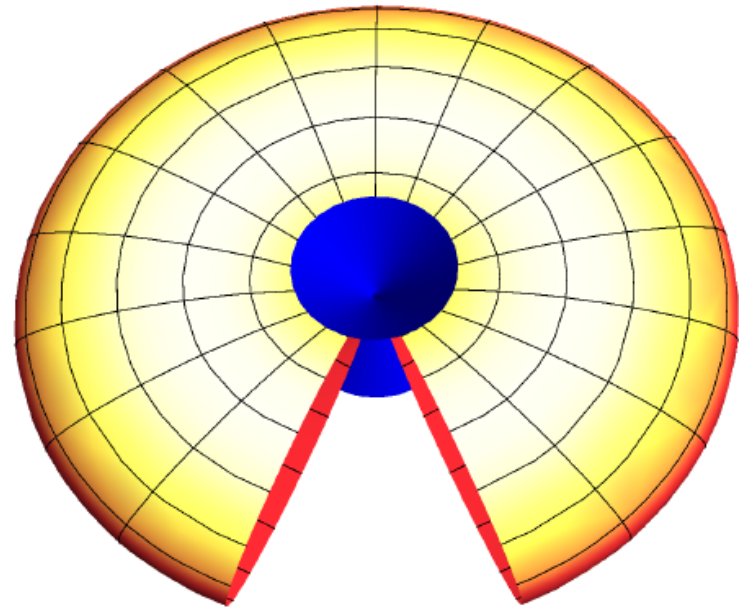
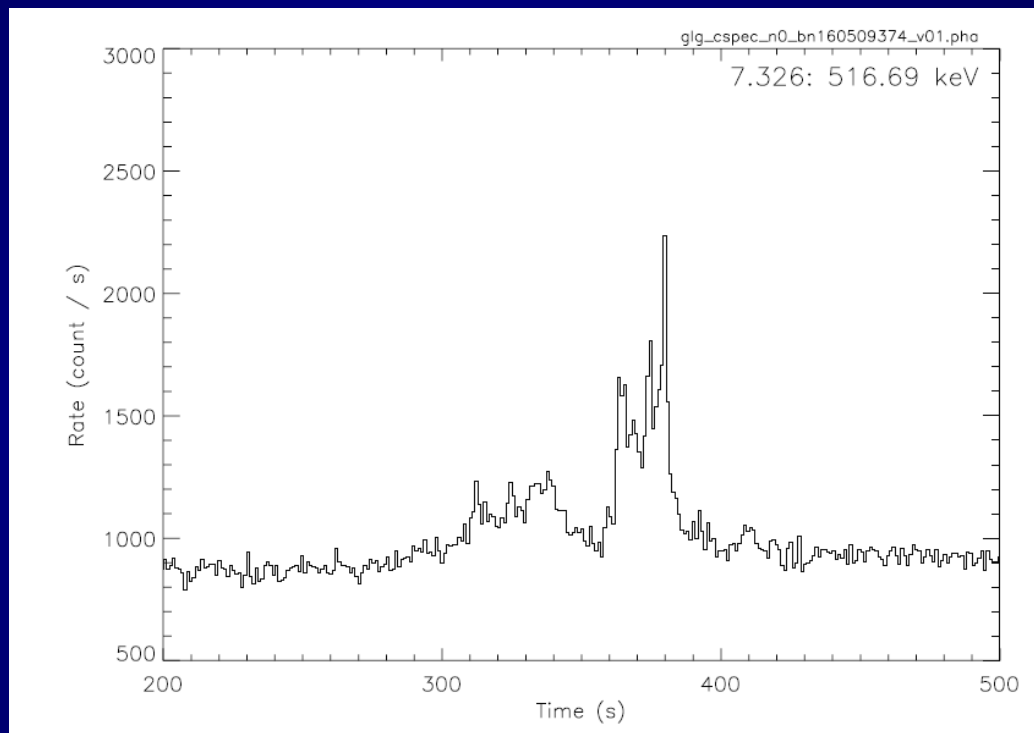
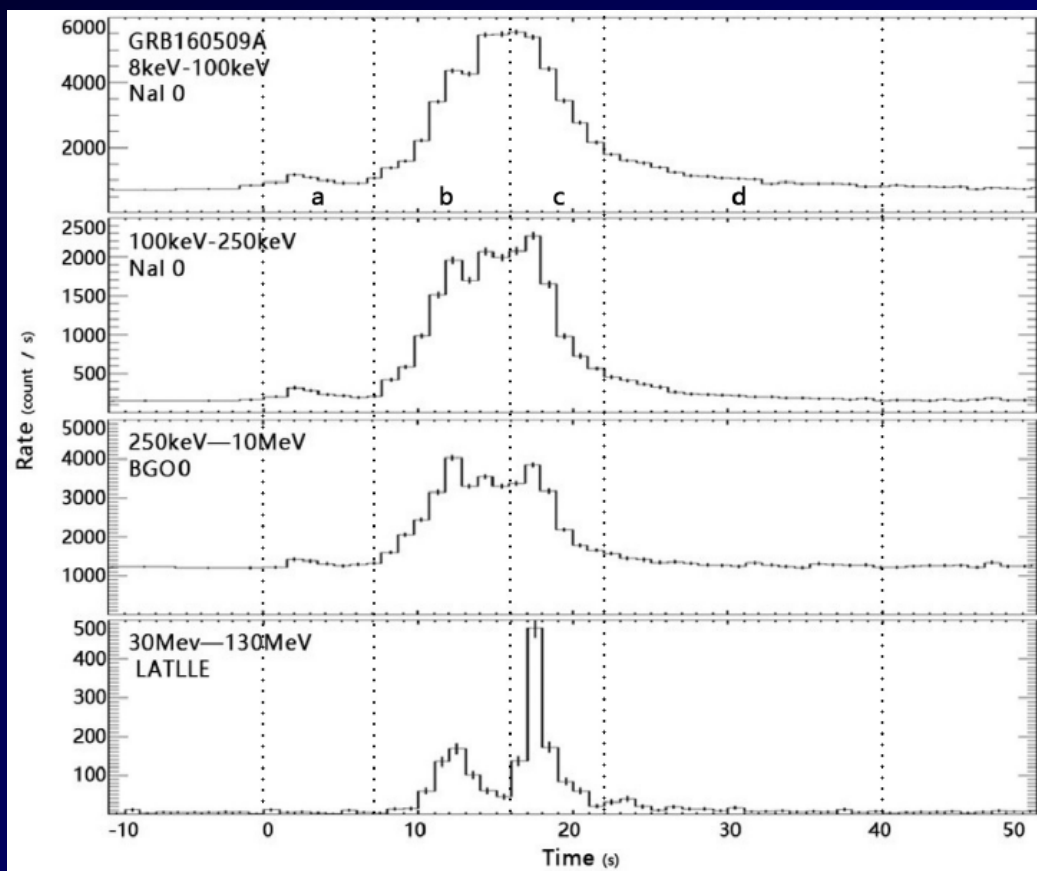


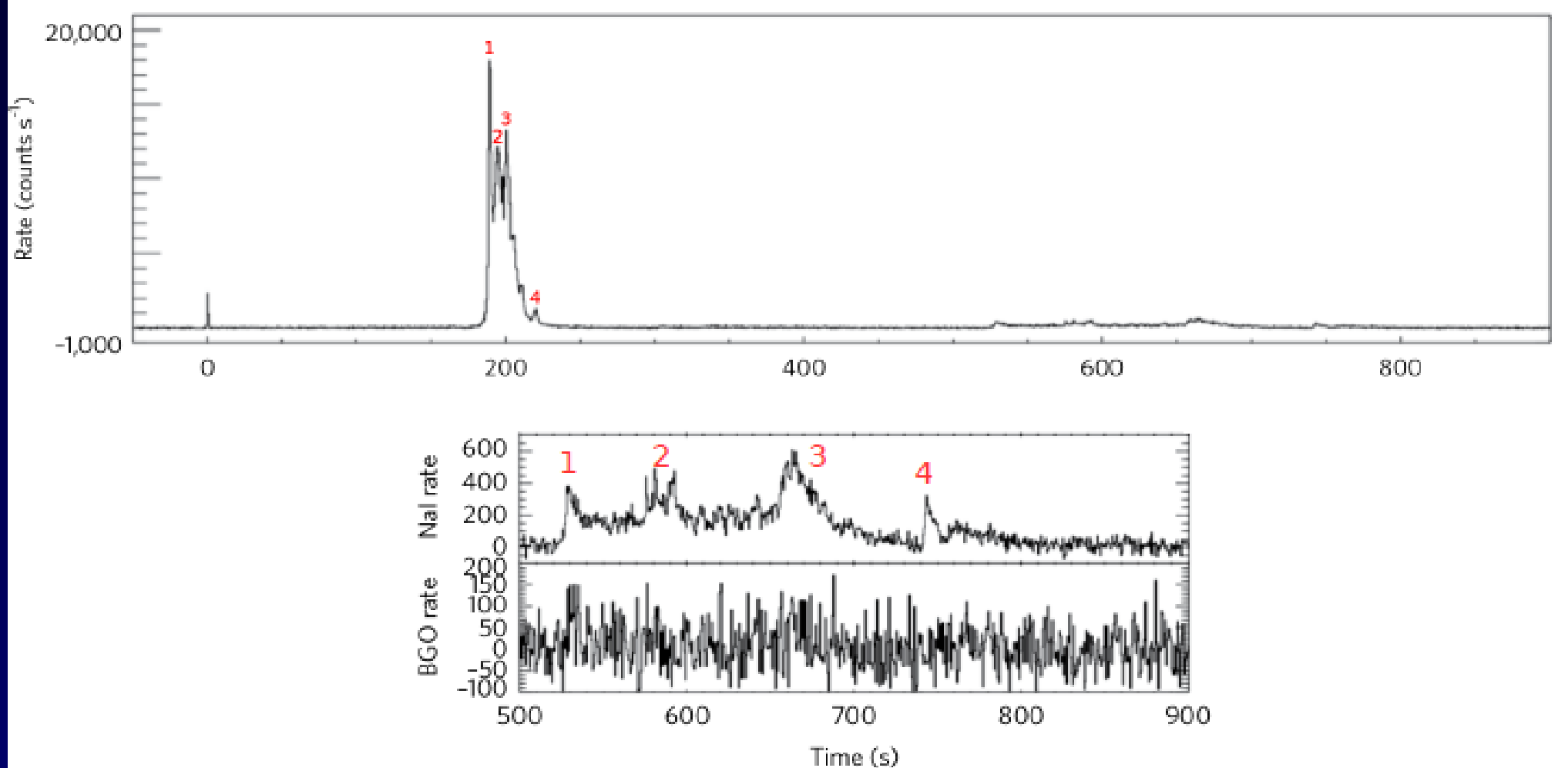
Figure 4. Idealized plot for showing the morphology of the BdHNe. The GeV emission is detectable when the viewing angle is less than the 55.77° from the normal to the orbital plane. Left panel is the situation in which the detectors can observe the GeV emission and the right panel is the one which GeV emission is not detectable and only Gamma-ray and X-ray flares are detectable.

An analogy between GRBs and AGNs

A prescient polar view of a BdHN: GRB 160509A

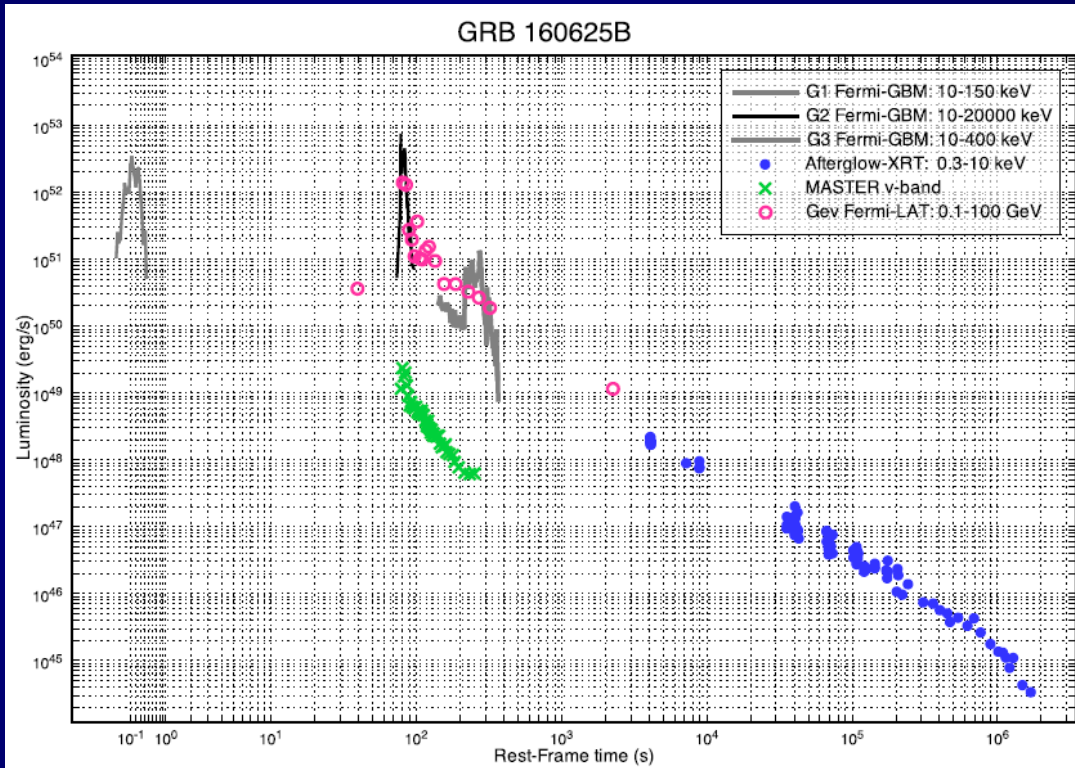
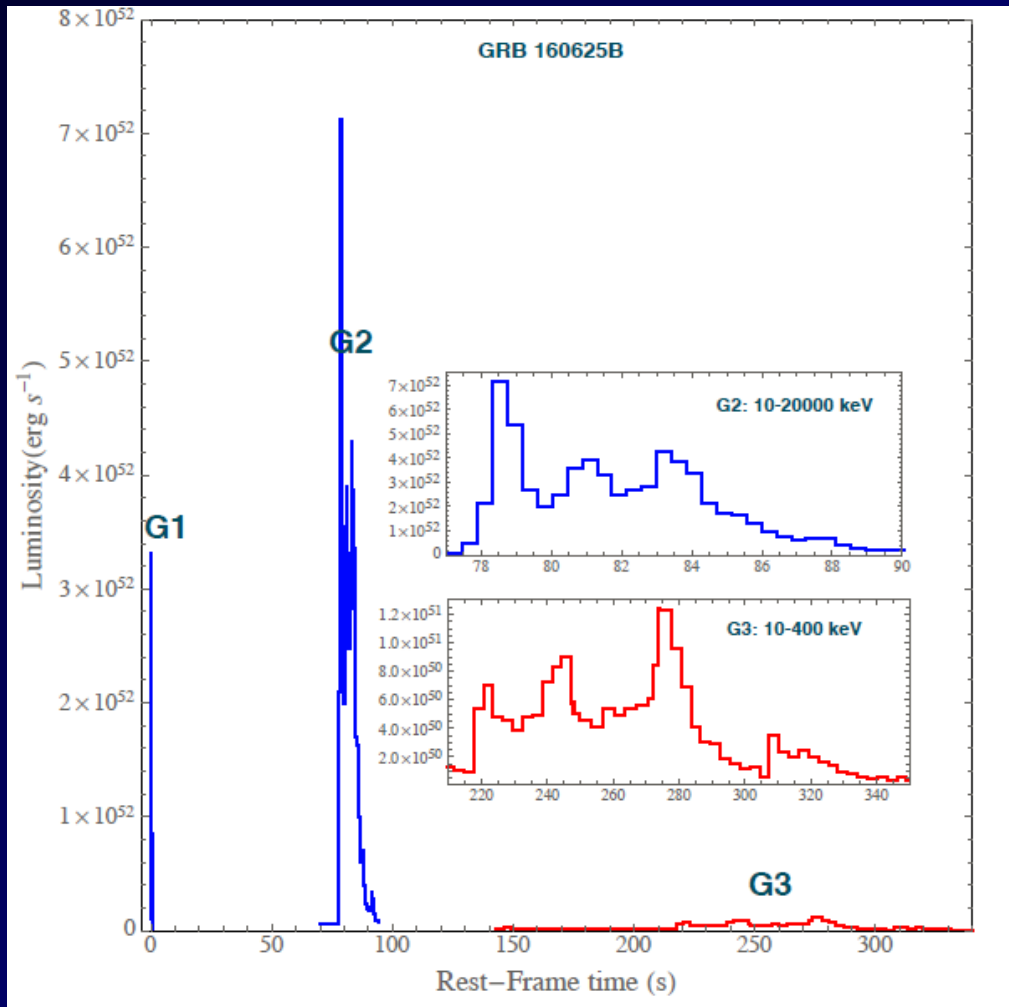


A current polar view of a BdHN



Data from B.-B. Zhang et. al., Nat. Astron. 2017
See D. Melon-Fuksman talk for the source BdHN interpretation

A current polar view of a BdHN



Data from B.-B. Zhang et. al., Nat. Astron. 2017
Analysis by R. Moradi; see his talk in GB11 session for details

Conclusion

The interpretation of GRB phenomenology
cannot overlook the knowledge of the
morphology of the binary progenitors

The Planck Mass (m_p)

$$\frac{\hbar}{mc} \quad \frac{Gm}{c^2}$$
$$m_p = \left(\frac{\hbar c}{G}\right)^{1/2}$$

The Critical Mass of Black Hole

Fermions

$$M_{crit}^F = \frac{m_p^3}{m^2}$$

Bosons

$$M_{crit}^B = \frac{m_p^2}{m^2}$$

$$M_{BH} > M_{crit}^{F,B}$$

Thanks to...

**Y. Aimuratov, L. Becerra, D. Begue, R. Belvedere, M.G. Bernardini,
C.L. Bianco, L. Caito, R. Camargo, P. Chardonnet, C. Cherubini, F.
Cipolletta, A. Corsi, M.G. Dainotti, T. Damour, G. De Barros, M.
Enderli, S. Filippi, F. Fraschetti, C. Fryer, R. Guida, L. Izzo, M.
Karlica, R. Kerr, M. Kovacevic, L. Li, G. Mathews, J.D. Melon
Fuksman, R. Moradi, M. Muccino, F. G. Oliveira, B. Patricelli, A.V.
Penacchioni, G.B. Pisani, G. Preparata, D. Primorac, L.J. Rangel
Lemos, J.F. Rodriguez, M. Rotondo, J. Rueda, J. Salmonson, S.
Shakeri, I. Siutsou, G. Vereshchagin, Y. Wang, J. Wilson, S.-S. Xue,
E. Zaninoni.**